A TWO-COMPONENT RAIN MODEL FOR THE PREDICTION OF ATTENUATION AND DIVERSITY IMPROVEMENT

by

Robert K. Crane

Thayer School of Engineering
Dartmouth College
Hanover, New Hampshire 03755

February 1982

Prepared for

Environmental Research & Technology, Inc.

Under their Contract NASW-3506

with the

National Aeronautics and Space Administration

Washington, D.C.

ABSTRACT

A new model was developed to predict attenuation statistics for a single earth-satellite or terrestrial propagation path. The model was extended to provide predictions of the joint occurrences of specified or higher attenuation values on two closely spaced earth-satellite paths. The joint statistics provide the information required to obtain diversity gain or diversity advantage estimates.

The new model is meteorologically based. It was tested against available earth-satellite beacon observations and terrestrial path measurements. The model employs the rain climate region descriptions of the Global rain model. The rms deviation between the predicted and observed attenuation values for the terrestrial path data was 35 percent, a result consistent with the expectations of the Global model when the rain rate distribution for the path is not used in the calculation. Within the United States the rms deviation between measurement and prediction was 36 percent but worldwide it was 79 percent.

ACKNOWLEDGEMENT

The author wishes to acknowledge the help of his daughter, Cindy, in providing some of the pocket calculator calculations of slant path attenuation statistics needed to check the computer runs. He also wishes to acknowledge the help of D. Blood while at the Environmental Research & Technology, Inc. in the preparation of the table of coefficients representing the rain climate zone rate distribution.

TABLE OF CONTENTS

LIST OF ILLUSTRATIONS

LIST OF ILLUSTRATIONS (cont.)

A TWO-COMPONENT RAIN MODEL FOR THE PREDICTION OF ATTENUATION AND DIVERSITY IMPROVEMENT

1. INTRODUCTION

Attenuation due to rain has long been recognized as a major limitation to reliable communication system operation at frequencies above 10 GHz (e.g. Crane 1971, 1977). The large fade margins required for satisfactory system performance at all but the extremely small percentages of time demanded by many system users are expensive if not impossible to achieve. One of the methods proposed for the mitigation of the effects of attenuation on communication system performance employs space or path diversity (Hogg 1967, Allnutt 1978, Lin et al. 1980). Communication is effected by two or more spatially separated paths with the expectation that severe attenuation will affect only one of the paths at a time. Information required for diversity system design includes the expected attenuation statistics for a single path and the joint statistics for two (or more) spatially separated paths simultaneously suffering the same or higher attenuations. In this paper, a new model is presented for the prediction of both single and joint path attenuation statistics for use in system design.

A number of attenuation prediction models are available for the calculation of attenuation statistics for a single

path (e.g. Ippolito et al. 1981, Crane 1980, Dutton et al. 1982, Fedi 1981, Goldhirsh 1982, Lin 1977, Persinger et al. 1980). The models are of two general types; one of which relies on rain gauge or radar observations to adjust attenuation statistics observed on one path for prediction on another path; the other employs meteorological information about the intensity and spatial structure of rain to effect the prediction. Most of the models rely on the adjustment of attenuation observations. The "Global" model developed by Crane (1980) and the "Two-Component" model presented in this paper are examples of the latter type. Both types of models are necessary. The former tends to be more accurate for prediction in similar climate regions, propagation geometries, and within narrow frequency limits. The latter are required for application in different climate regions, for different geometries and over wide frequency limits.

Several models are available for the prediction of the improvement to be gained by the use of space diversity (Ippolito et al. 1981, Hodge 1976, Goldhirsh 1981). These are of the former type based either on spaced-path measurements or on radar simulations of such measurements. The Two-Component model provides a meteorologically based prediction method which includes the effects of varying the base line length and orientation relative to the direction of the

propagation path, the frequency and the climate region. The application of the new model has revealed a wider range of diversity improvement results than predicted by the earlier models. Available diversity observations are consistent with the predicted wider range of possible results.

Both the single path and joint path predictions of the Two-Component model were compared with available observations using a modification of the attenuation ratio method recommended by the CCIR (1982a) and by an equivalent probability ratio method. A measure of the efficacy of the new model was obtained by comparison with the results of a similar measurement and model analysis employing the recently developed CCIR attenuation prediction procedure (CCIR 1982b; Fedi 1980).

Terrestrial path data from measurements on 36 paths at frequencies from 7 to 82 GHz and path lengths from 1.3 to 58 km were used to test the Two-Component (and CCIR) model. Twenty-nine of the paths were from 10 separate locations in western Europe. The new Two-Component model predicted the attenuation values observed in the 0.1 to 0.001 percent of the year probability range with an rms deviation of 35 percent. The CCIR model predicted the observed attenuation values with a 17 percent deviation. These values are within the expected 20 percent rms error for prediction when the rain rate distribution at a location is known (CCIR model) or the 40

percent error when only the rain climate region is specified (Two-Component model; see Crane 1980 or CCIR 1982a). The observed probability deviations were larger than the attenuation deviations. The Two-Component model predicted the probability values at a set of fixed attenuation levels with a 145 percent rms error while the CCIR model predicted the probability values with a 49 percent error.

The two models were also compared using available satellite beacon data. Data from 47 paths were available for testing the Two-Component model, 17 in the United States, 10 in Europe, and 20 in Japan; data from only 31 of the 47 paths included the point rain rate information required for the CCIR model, 9 in the United States, 4 in Europe and 18 in Japan. The beacon measurements were made at latitudes ranging from 24 to 53°N, within a 11.6 to 34.5 GHz frequency range. The Two-Component model predicted the observed attenuation values to within an error of 79 percent; the CCIR model predicted the attenuation values to within 58 percent. The observed probability values were predicted by the Two-Component model to within 142 percent while the CCIR model had an error of 166 percent.

Only a limited amount of data were available for testing the efficacy of the Two-Component model for the prediction of the joint statistics for space diversity paths. Low elevation angle satellite beacon observations made at

Blacksburg (Towner et al.) at 11.6 GHz compared favorably with the model predictions. The calculated deviation was less than 6.5 percent for a baseline of 7.3 km. Comparison with the radar simulations presented by Goldhirsh (1981) show good agreement for baselines shorter than 10 km but poor agreement for longer baselines. Comparison with the radiometer observations on 18-20 km baselines presented by Strickland (1978) show model predictions of better than observed diversity performance. Similarly, the 19 GHz diversity observations made with the Tampa Triad (Davidson and Tang 1982) show a progressive increase in prediction error with increasing baseline. The percent deviation between predicted and observed attenuation values ranged from 42 percent for an 11 km baseline to 366 percent for a 20 km baseline.

The new Two-Component model performs well for the prediction of single site attenuation statistics and for diversity statistics for baselines shorter than about 15 km. For longer baselines, the prediction errors increase. A number of model improvements are possible for the longer baseline situation but additional weather radar observations are needed first to provide the data required for the extension of the model.

2. THE TWO-COMPONENT MODEL

The Two-Component model for the prediction of attenuation due to rain, separately addresses the contributions of rain showers and the larger regions of lighter rain fall surrounding the showers. Some of the earlier models for the prediction of the statistics of point rainfall rates, such as the model developed by Rice and Holmberg (1973), recognized the differences between convective or thundershower rain and widespread or stratiform rain. Separate roles for thunderstorm and stratiform rain as different rain types were maintained through the continued development and use of that model for attenuation prediction (Dutton and Dougherty 1973, Dutton et al. 1982). The statistical prediction procedures developed by Misme and Fimbel (1975) for application to terrestrial paths and by Misme and Waldteufel (1980) for application to earth-space paths depended upon the separate accounting for the effects of rain within cells and within the wider, lower intensity rain region surrounding the cells. In their models, a cell was required for the occurrence of attenuation whether the rain type was classified as convective or widespread.

Weather radar observations show that rain is always spatially inhomogeneous with cells occurring in all rainfall types. Figure 1a displays the familiar pattern of occurrence of cells in a convective shower. Figure 1b depicts the

attenuation values calculated from the radar reflectivity observations (Figure 1a) for an azimuth scan through the shower at an elevation angle of 1.4°. Simultaneous radiometer observations showed that the attenuation calculations were correct (Crane 1971). The cell contributions to the attenuation are evident. The reflectivity peaks - volume cells (Crane 1979) - are darkened in Figure 1a. The darkened areas - volume cells - correspond to three dimensional regions of a storm with reflectivity values within 3dB of their local peak values. The horizontal area of a volume cell is small. The largest of the six volume cells depicted in Figure 1a has a maximum horizontal dimension of less than 3 km. The more extensive region of rain debris (within the 20 dBZ contour) surrounding the volume cells contributes little to the attenuation when the propagation path traverses a volume cells but produces all the attenuation for a path which does not intersect a volume cell. The term "volume cell" is used to refer to the small volume surrounding a local reflectivity peak which has reflectivity values greater than one half the peak value. The term "debris" is used to refer to the larger region of lighter rain rate surrounding a volume cell. Many different cell definitions have been used and the modifier - volume - is employed to specify the quantitative definition of a radar-observed cell used in this analysis.

The Two-Component model handles the cells - volume

cells defined by the region within 3dB of local reflectivity maxima - and the debris independently. All storms contain volume cells and debris but propagation paths through the rain do not always intersect a single, isolated volume cell. For example, Path A in Figure 1a and 1b does not intersect a cell and propagation paths through volume cells 1 and 2 or through volume cells 3, 4 and 5 intersect more than one volume cell. In each of the latter cases the volume cell at a closer range had a reflectivity value of 5 or more dB below the peak value of the dominant volume cell and the effect of the second volume cell could be neglected when compared with the effect of the dominant volume cell. The Two-Component model assumes either a single volume cell or only debris along a path. The model is designed for the calculation of the probability that a specified attenuation level is exceeded. One of the two-components of the rain process, a volume cell or debris, may produce the attenuation value. The probability associated with each component is calculated and the two values are summed to provide the desired probability estimate.

2.1 Point Rain Rate Distribution

The Global attenuation prediction model (Crane 1980) provided empirical descriptions of the probability distributions of point-surface rainfall rate to be expected anywhere within a rain climate region. A revised version of the Global model

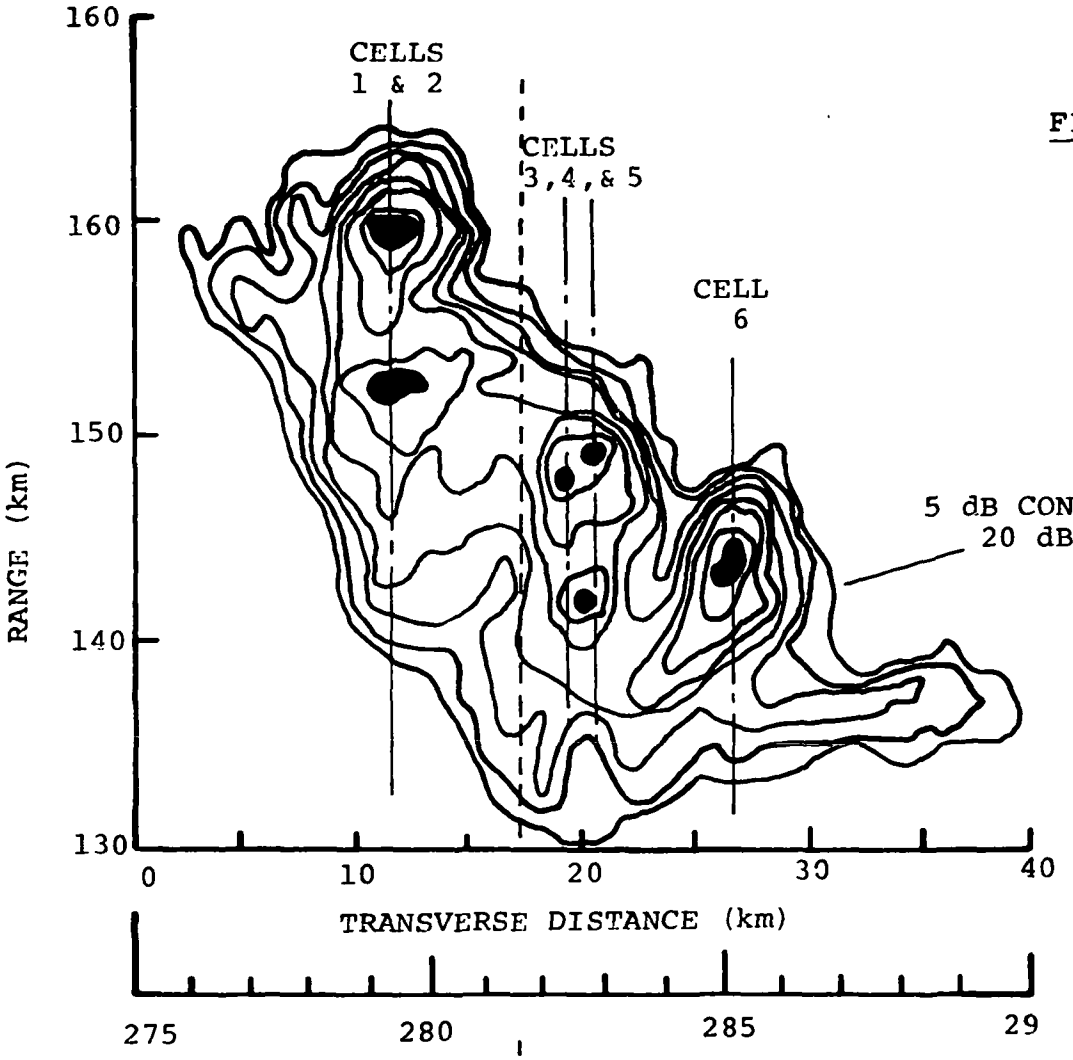

FIGURE 1a.

FIGURE 1b.

7.8 GHz

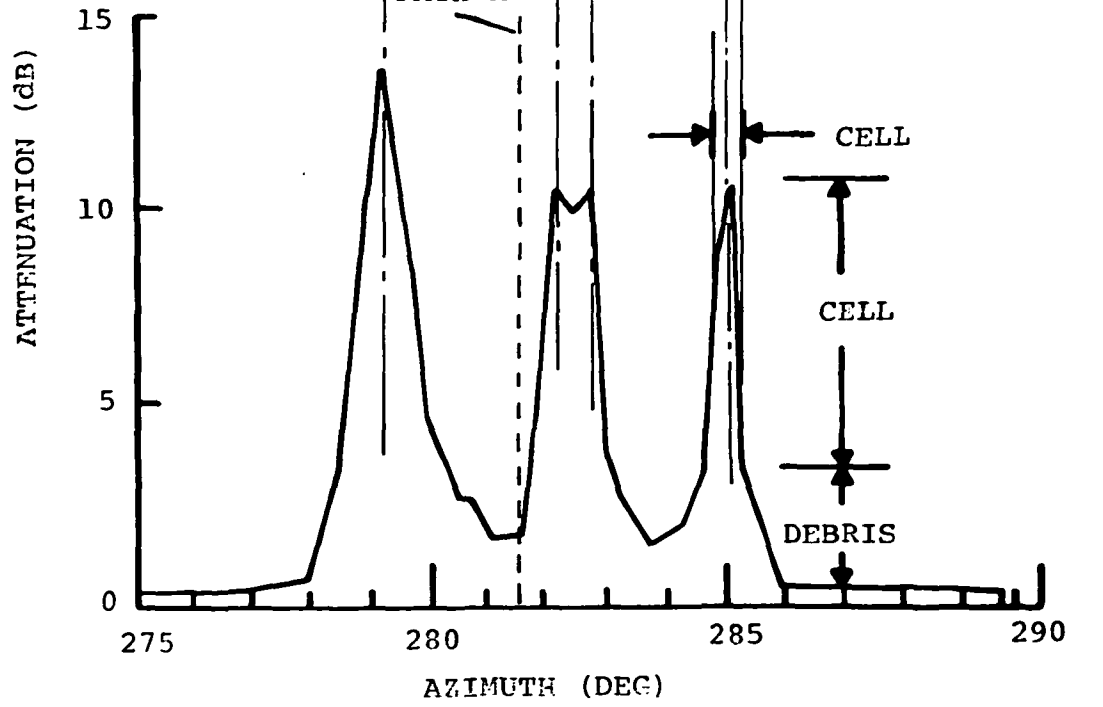

rain climate region map for the continental United States is displayed in Figure 2. The major difference between this and the earlier map is the division of rain climate region B into 2 sub-regions, B1 and B2 and an adjustment of the contour region boundaries near the Canadian border to accomodate the extensive set of rain rate distribution measurements published by Segel (1979). A revised map for western Europe is presented in Figure 3. In this case, the map was redrafted to represent the larger rain rate distribution data base prepared as a part of the EUROCOP-COST 25/4 Project (Fedi 1979).

The rain climate region boundaries were initially established using climatological and topographical data. The data were used to define regions for pooling or combining available rain rate distribution observations for estimating a single, best estimate empirical distribution function for the region. With the increased number of rain rate distribution observations now available, some adjustment in climate region boundaries and in the empirical distributions is to be expected. The Global model empirical distribution functions were also extended to span the 0.0001 to 10 percent of the year range where data were available. The new distribution functions were constrained to produce, when integrated, the observed average annual rain accumulation (depth) for each rain climate zone.

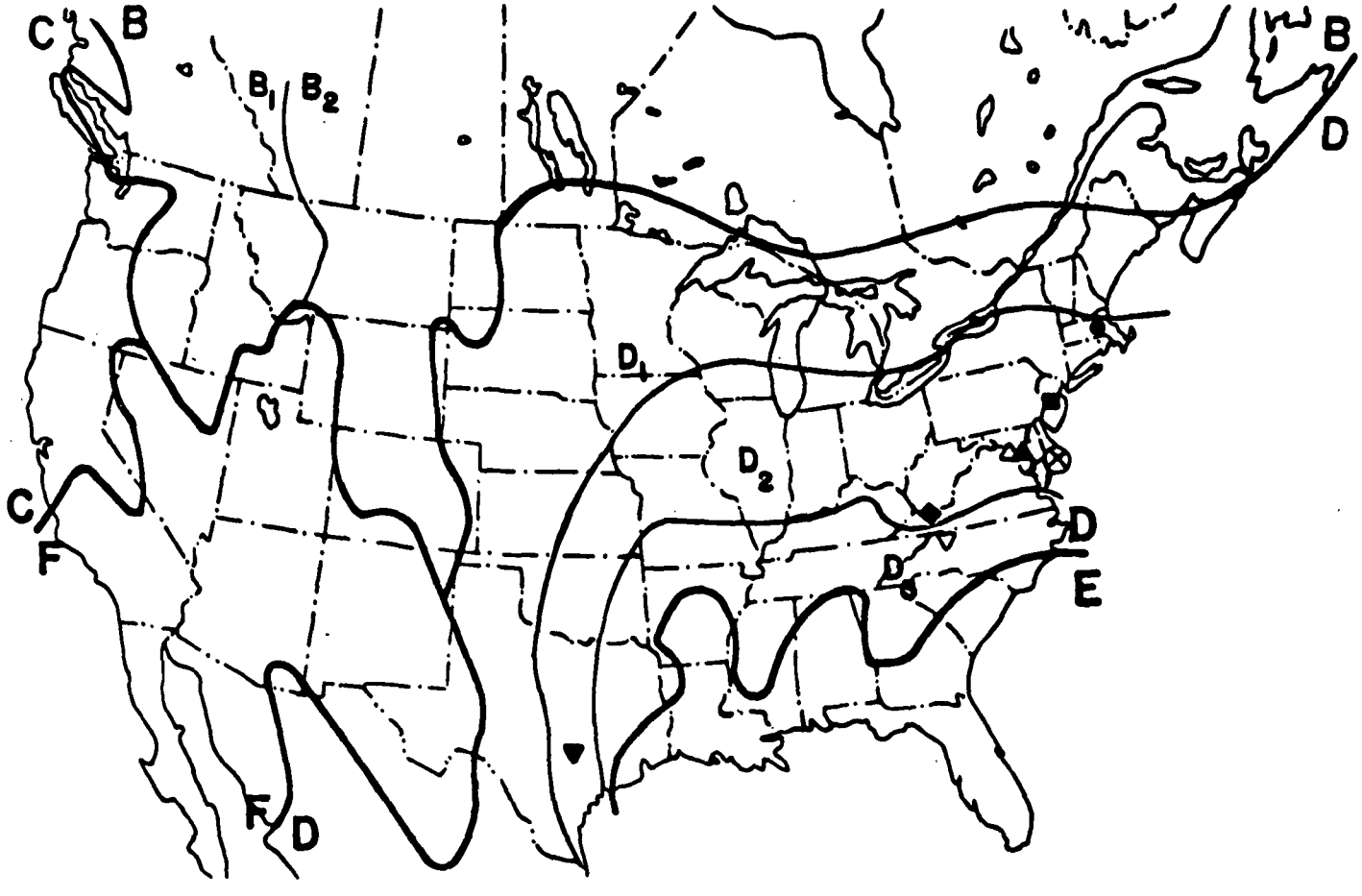

LOCATIONS USED FOR SLANT PATH MEASUREMENTS

- ● WALTHAM, MASS.
- ■ HOLMDEL, N.J.
- ▲ GREENBELT, MD.
- △ CLARKSBURG, MD.
- ◆ BLACKSBURG, VA.
- ▽ ROSMAN, N.C.
- ⊗ WALLOPS ISLAND, VA.
- ▼ AUSTIN, TEX.

FIGURE 2.

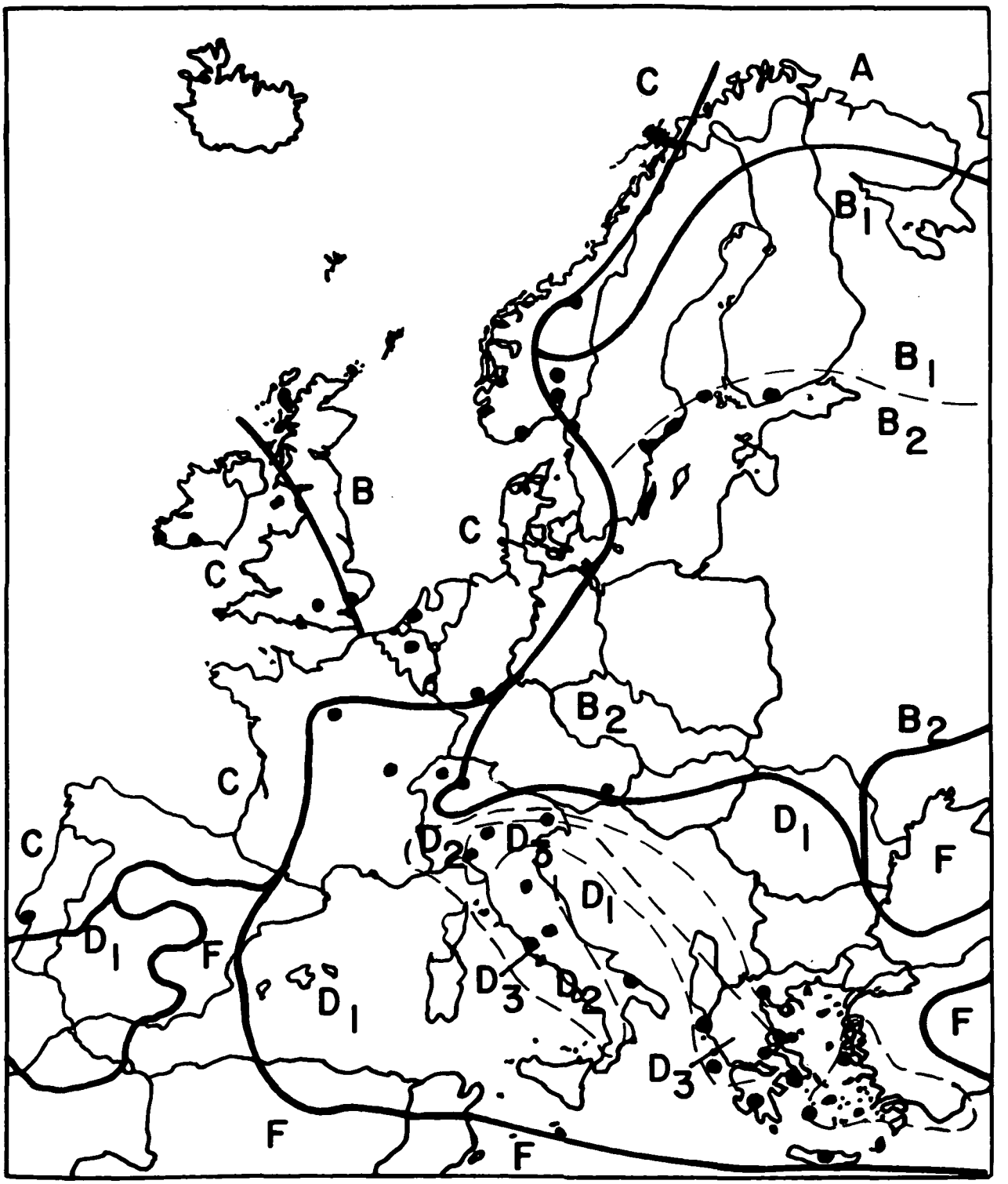

FIGURE 3.

Results from a three year radar measurement program in Goodland, Kansas were used to establish the detailed descriptions of the volume cells and debris regions required for the attenuation. Average volume cell parameters were obtained from observations of over 240,000 volume cells gathered from a 25 storm day sample from the 3 year observation set (Crane and Hardy 1980). The average diameter of a circular cell with the horizontal area of the volume cell at the height of peak reflectivity is depicted in Figure 4, and the average vertical extent is depicted in Figure 5. Figure 5 also displays the average height of the highest detected element of a volume cell (summit; see Crane 1979). The distributions of volume cell area and of volume cell lifetime were found to be exponential (Crane 1979).

The rain occurring over a rain gauge was modeled to arise from either a volume cell or from the debris surrounding a volume cell. For the 25 storm days, the contribution of the volume cells in the 240,000 cell sample could be calculated based on the area, reflectivity, and lifetime data for the volume cells and on the surveillence area and scanning strategy of the radar. The volume cells produced the rain rate distribution shown in Figure 6. For display in this figure, the observed occurrence probabilities for the volume cell component were adjusted by the ratio of the annual D1 region accumulation to the radar observed

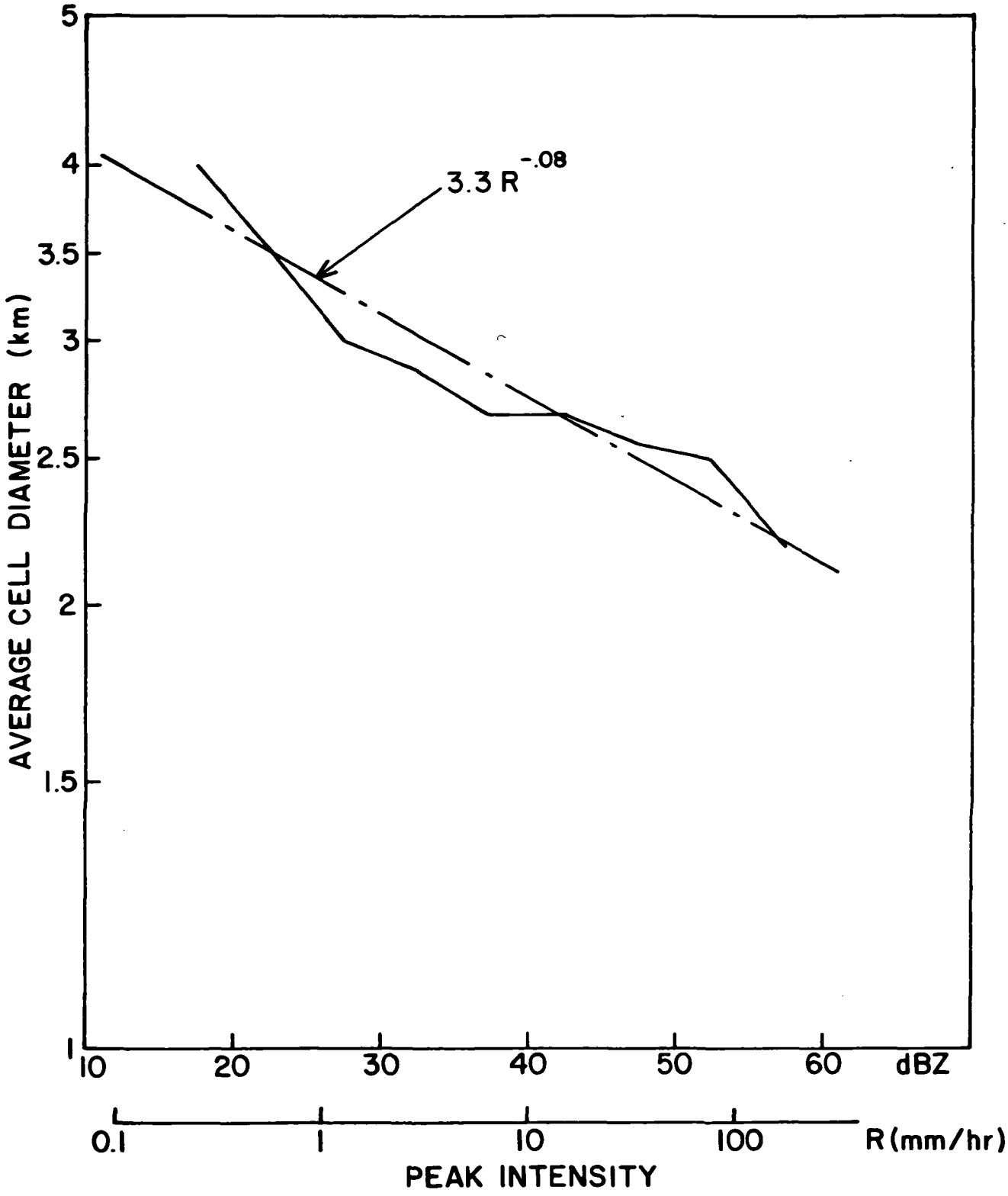
5
4
3.5
3
2.5
2
1.5
1
AVERAGE CELL DIAMETER (km)
3.3 R^-.08
10
20
30
40
50
60
dBZ
0.1
1
10
100
R(mm/hr)
PEAK INTENSITY

FIGURE 4.

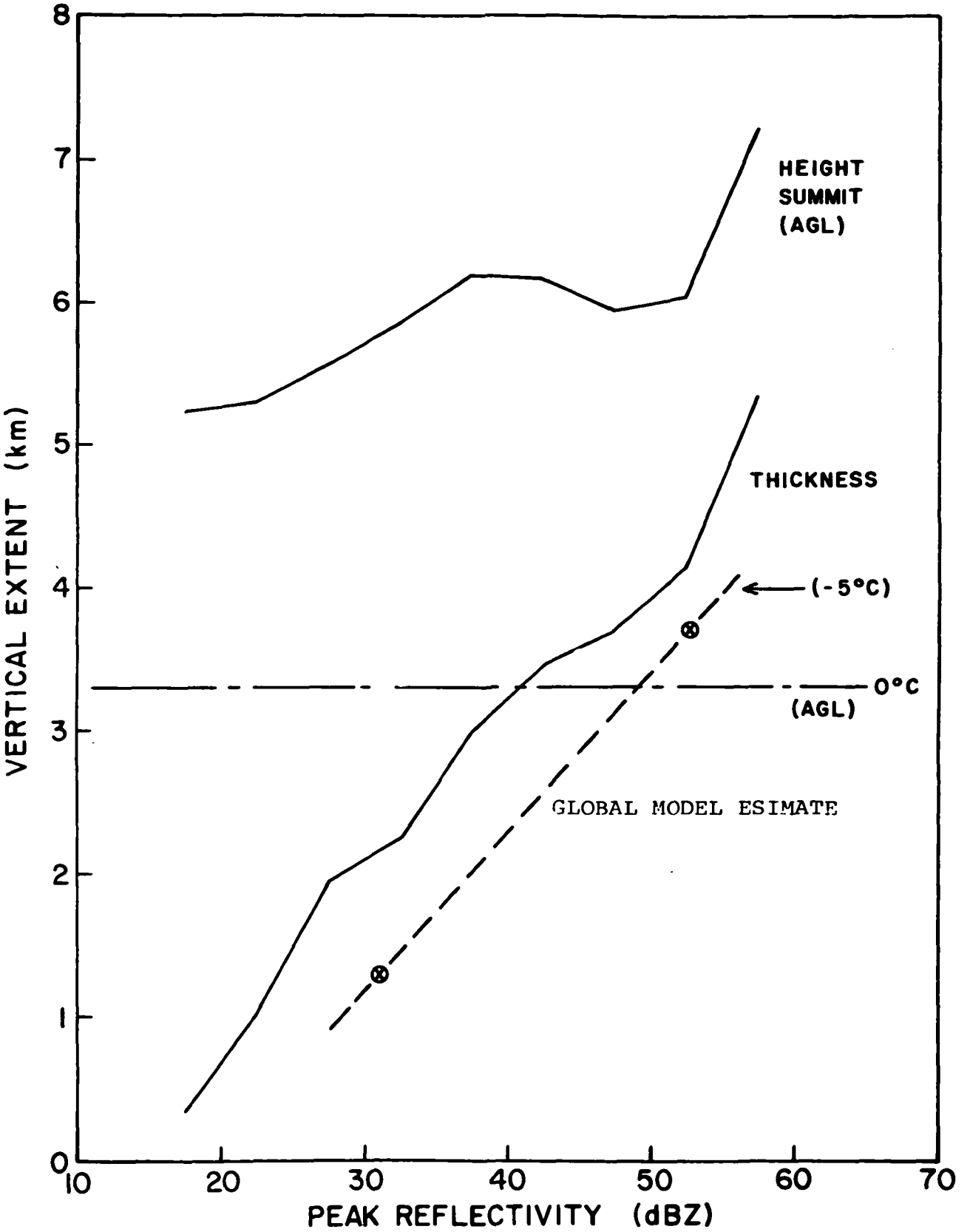
VERTICAL EXTENT (km)
PEAK REFLECTIVITY (dBZ)
HEIGHT SUMMIT (AGL)
THICKNESS
(-5°C)
0°C (AGL)
GLOBAL MODEL ESIMATE
0
1
2
3
4
5
6
7
8
10
20
30
40
50
60
70

FIGURE 5.

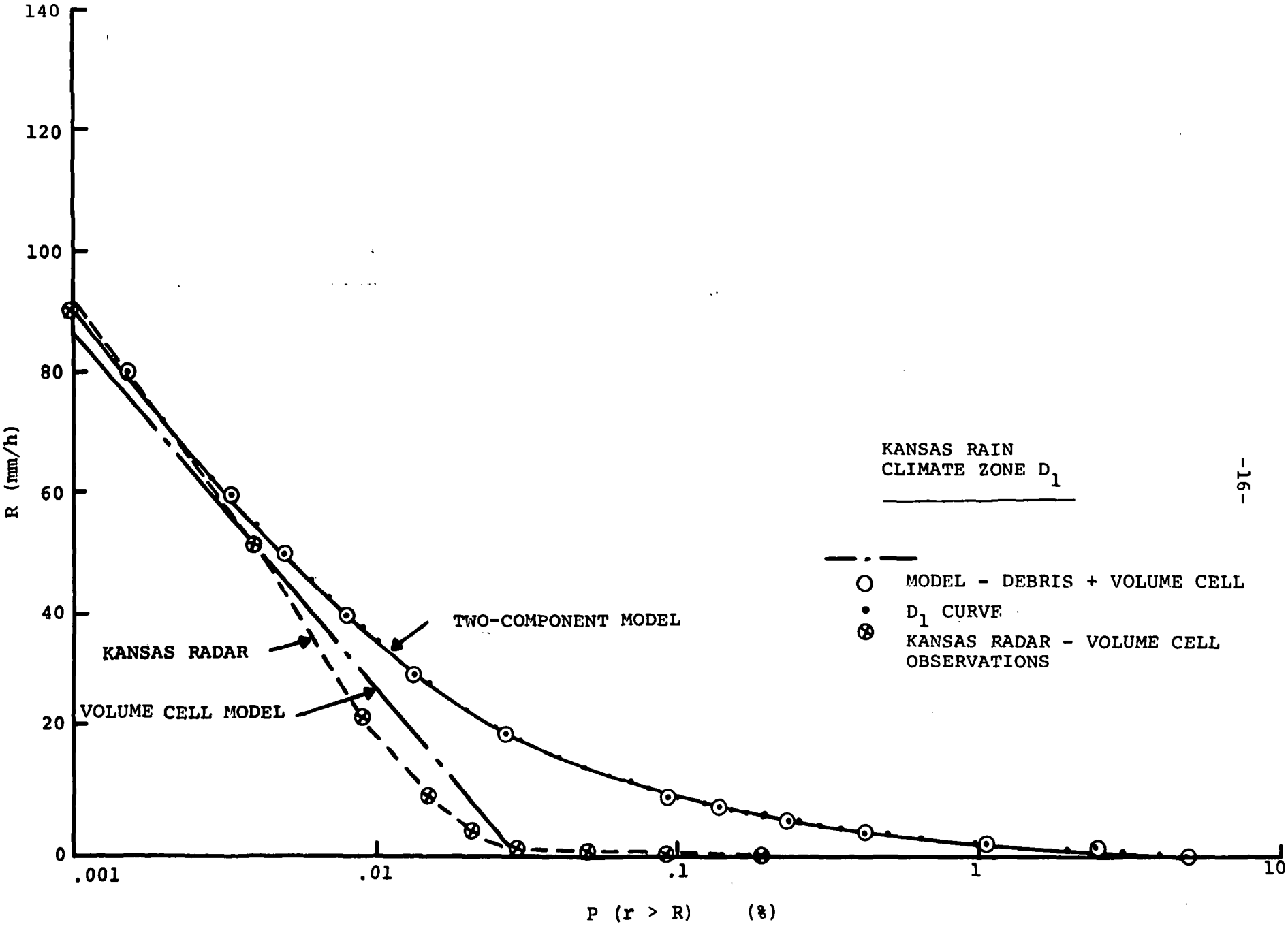
140
120
100
80
60
40
20
0
R (mm/h)
.001
.01
.1
1
10
P (r > R) (%)
KANSAS RAIN
CLIMATE ZONE D_1
MODEL - DEBRIS + VOLUME CELL
D_1 CURVE
KANSAS RADAR - VOLUME CELL OBSERVATIONS
TWO-COMPONENT MODEL
KANSAS RADAR
VOLUME CELL MODEL

FIGURE 6.

total accumulation averaged over the surveillence area of the radar for the 25 storms. This scaling was necessary for combining the radar data with the Kansas - region D1 - distribution function estimate. From this figure, it is evident that the volume cells contribute little to the total accumulation but are responsible for most of the precipitation at rain rates above 30 mm/h and all the precipitation at rates above 70 mm/h. Calculation showed that less than 10 percent of the total accumulation was produced by the volume cells. The rain region surrounding a 70 mm/h volume cell could produce debris with a rate in excess of 30 mm/h.

A simple approximation to the observed, volume-cell produced rain rate distribution is an exponential distribution as illustrated by the volume-cell-model curve in Figure 6. The portion of the empirical D1 region distribution function not accounted for by the exponential volume cell component distribution is attributed to rain debris. The debris distribution function was nearly log-normal over its entire range, 0.001 to 5 percent of the year. Using the rain rate values in the 0.1 to 10 mm/h range, a log-normal distribution function was fit to the D1 region curve. The resultant average of the natural logarithm of the rain rate was -0.2 corresponding to a rain rate of 0.83 mm/h and the standard deviation was a factor of 3.1. The average rain rate (predominantly debris,

calculated by averaging the logarithm of the rain rates) observed by the radar was 0.8 mm/h and the standard deviation was a factor of 2.8, nearly identical with the debris distribution parameters inferred from the D1 distribution.

The sum of the independent volume cell and debris distributions, the former exponential and the latter log-normal, exactly represented the empirical D1 distribution function as shown in Figure 6. A combination of an exponential plus a log-normal distribution was found also to fit precisely the empirical distribution functions for the other rain climate regions.

The Two-Component model for the empirical rain rate distribution functions is

$$P(r \geq R) = P_c(r \geq R) + P_D(r \geq R) \quad (1)$$

$$P_c(r \geq R) = P_c e^{-R/R_c} \quad (2)$$

$$P_D(r \geq R) = P_D \, \eta \left(\frac{\ell nR - \ell nR_D}{\sigma_D}\right) \quad (3)$$

where $P(r \geq R)$ is the probability that the observed rain rate, r, exceeds the specified rain rate, R, (percent). $P_c(r \geq R)$, $P_D(r \geq R)$ are the distribution functions for cells and debris respectively, (percent). r, R are rain rates (mm/h), P_c is the probability of a cell (percent), R_c is the average cell rain

rate (mm/h), η is the normal distribution function, ℓn is the natural logarithm, P_D is the probability of debris (percent), R_D is the average rain rate in the debris (mm/h, calculated from the average of the logarithm of rain rate), and σ_D is the standard deviation of the logarithm of the rain rate.

The parameters for the model, P_C, R_C, P_D, R_D and σ_D for each fo the Global model rain climate zones are listed in Table I. Table I also includes a listing of the rain rate expected to be exceeded 0.01 percent of the year.

2.2 Path Averaged Rain Rate

Either a volume cell or the rain debris can produce rain along a line of rain gauges. The Two-Component model is used to predict the probability of occurrence of a specified or higher value of path averaged rain rate by independently summing the probabilities of a volume cell or of debris causing the observed path average value.

If a volume cell occurs over the path, the path integrated rain rate value is given by:

$$i = \int_0^D r(\ell)\,d\ell \qquad (4)$$

where i is the observed path integrated value (m^2/h), $r(\ell)$ is the rain rate profile along the path (mm/h) and D is the length of the path (Km).

The path integrated rain rate produced by a volume cell

TABLE I

Rain Zone	Cell Parameters P_C (%)	R_C (mm/h)	Debris Parameters P_D (%)	R_D (mm/h)	σ_D (mm/h)	R For $P(r \geq R) = 0.01\%$ (mm/h)
A	0.009	11.3	3.0	0.20	1.34	10
B_1	0.016	15.2	9.0	0.24	1.26	15
B	0.018	19.6	7.0	0.32	1.23	18
B_2	0.019	23.9	7.0	0.40	1.19	22
C	0.023	24.8	9.0	0.43	1.15	26
D_1	0.030	25.7	5.0	0.83	1.14	36
D_2	0.037	27.8	5.0	1.08	1.19	49
D_3	0.100	15.0	5.0	1.38	1.30	62
E	0.120	29.1	7.0	1.24	1.41	100
F	0.016	20.8	3.0	0.35	1.41	10
G	0.070	39.1	9.0	1.80	1.19	95
H	0.060	42.1	9.0	1.51	1.60	245

is approximated by:

$$I = \left(\frac{RW_c}{C}\right) \qquad (5)$$

where I is the path integrated rain rate (m^2/h), R is the peak rain rate in the cell (mm/h), $W_c = \sqrt{S_c}$ is the average dimension of a volume cell with area S_c (W_c - km, S_c - km^2) and C is an adjustment factor required by the definition of a volume cell.

The adjustment factor is included to represent the contribution of the debris close to a cell but outside the region enclosing the -3dB reflectivity value relative to the peak value (factor of 0.61 in rate rate). The often used Gaussian rain cell profile would require a factor of C = 0.68. The attenuation values plotted in Figure 1b are consistent with that value for the adjustment factor. The adjustment factor obtains when the path is much longer than the average volume cell width. If the path is shorter than W_c, the actual path length should be used for the calculation of I and the adjustment factor should be unity.

The rain rate within a volume cell required to produce the specified path integrated rain rate therefore is modeled by:

$$R = CI/L_c \qquad (6)$$

where L_c = minimum of D or W_c (km),

$$C = \frac{1 + 0.7(D - W_c)}{1 + (D - W_c)} \quad ; \quad (D - W_c) > 0$$

$$= 1 \quad ; \quad (D - W_c) \leq 0$$

The probability of occurrence of this or a higher rain rate at a single point is given by $P_c(r \geq R)$. The volume cell may occur anywhere along a path of length D. Assuming that only one cell can affect the path at any instant of time, the cell can occur at random anywhere along the path, and the random cell location distribution is uniform spatially, the probability of exceeding a specified path integrated rain rate is:

$$P_c(i \geq I) = (1 + D/W_c)P_c(r \geq R)$$

$$= (1 + D/W_c)P_c e^{-(CI/L_c R_c)} \qquad (7)$$

The point rainfall occurrence probability is multiplied by the ratio of the area over which a volume cell can affect the path to the area over which a cell can affect a point. The areas can be calculated only when the shapes of the volume cells are known. The volume cells were not adequately resolved by the Kansas (or most other) weather radar and only the area information was available. Furthermore, a range of volume cell area values were observed. To simplify the model, the volume cells were all assumed to have the same cross-sectional area. A circular region of influence for a volume cell around a point is most consistent with the assumed uniform spatial occurrence distribution for volume cells and no information about shape.

The average length of a line through a circular volume cell is given by:

$$\bar{\ell} = \frac{\sqrt{\pi}}{2}\sqrt{S_c} = 0.9\sqrt{S_c} \quad (8)$$

The area of influence of the volume cell about a point is S_c and, as shown in Figure 7 the area of influence of a circular volume cell about a line of length D is:

$$S_i = S_c\left(1 + \frac{2}{\sqrt{\pi}}\frac{D}{\sqrt{A_c}}\right) = S_c\left(1 + \frac{D}{\bar{\ell}}\right) \quad (9)$$

Since both the area and shape of the cell is uncertain, it is sufficient to approximate $\bar{\ell}$ by $W_c = \sqrt{S_c}$ yielding the expression given in equation (7). It is noted that a square cell oriented along the line will produce the same result as equation (9) with $\bar{\ell} = \sqrt{S_c} = W_c$ as illustrated in Figure 7.

The effect of the debris region on the path can only be calculated if a spatial scale, W_D, is associated with the rain within the debris. The Kansas radar observations also provided data on the relationship between average rain rate and area for isolated echo areas (rain regions completely within the surveillence area of the radar). The data were used to provide the desired relationship between W_D and the average rain rate in the debris. The observations are depicted in Figure 8. The regression line for area vs. rain rate provided the best

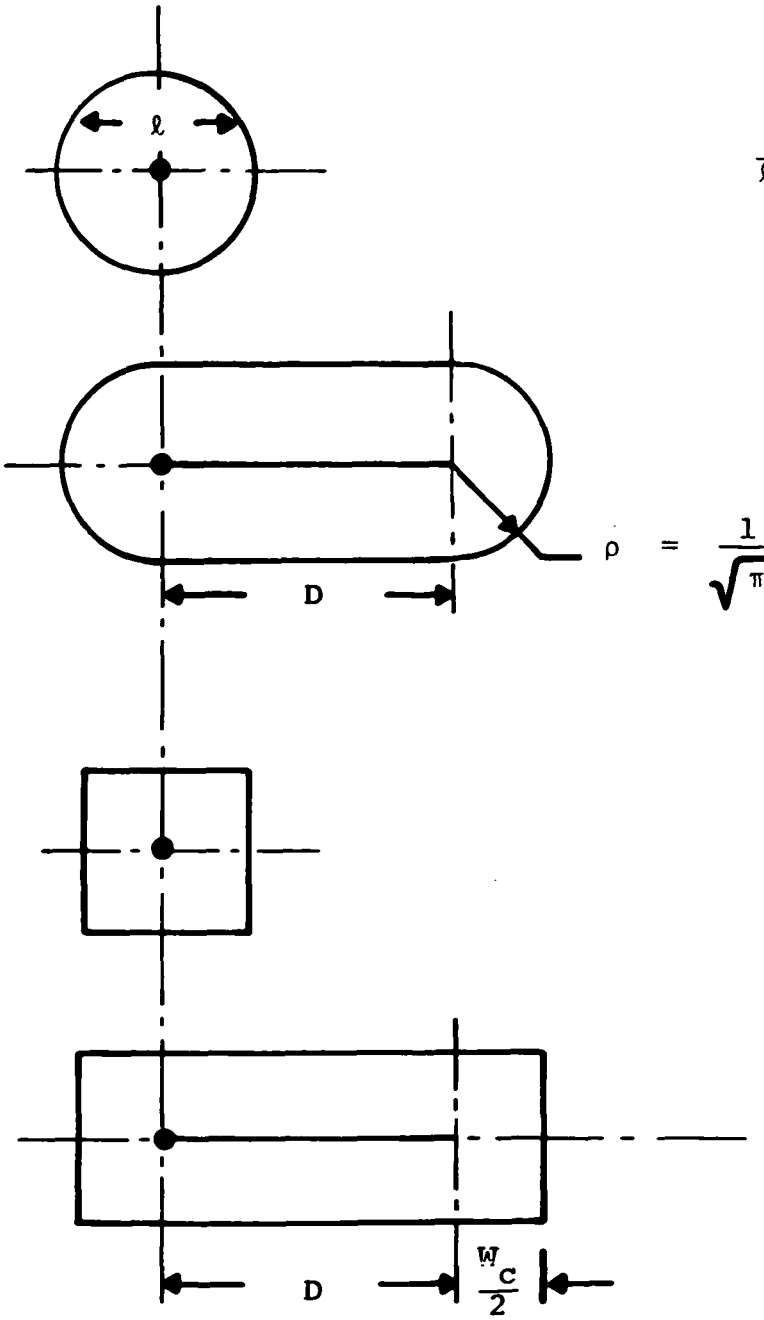

$$\bar{\ell} = \sqrt{\frac{\pi}{2}}\sqrt{S_c} = 0.9\ W_c$$

$$S_i = S_c\left(1 + \frac{D}{\bar{\ell}}\right) = S_c\left(1 + 1.13\ \frac{D}{W_c}\right)$$

$$\bar{\ell} = \sqrt{S_c}$$

$$S_i = S_c\left(1 + \frac{D}{\bar{\ell}}\right) = S_c\left(1 + \frac{D}{W_c}\right)$$

FIGURE 7.

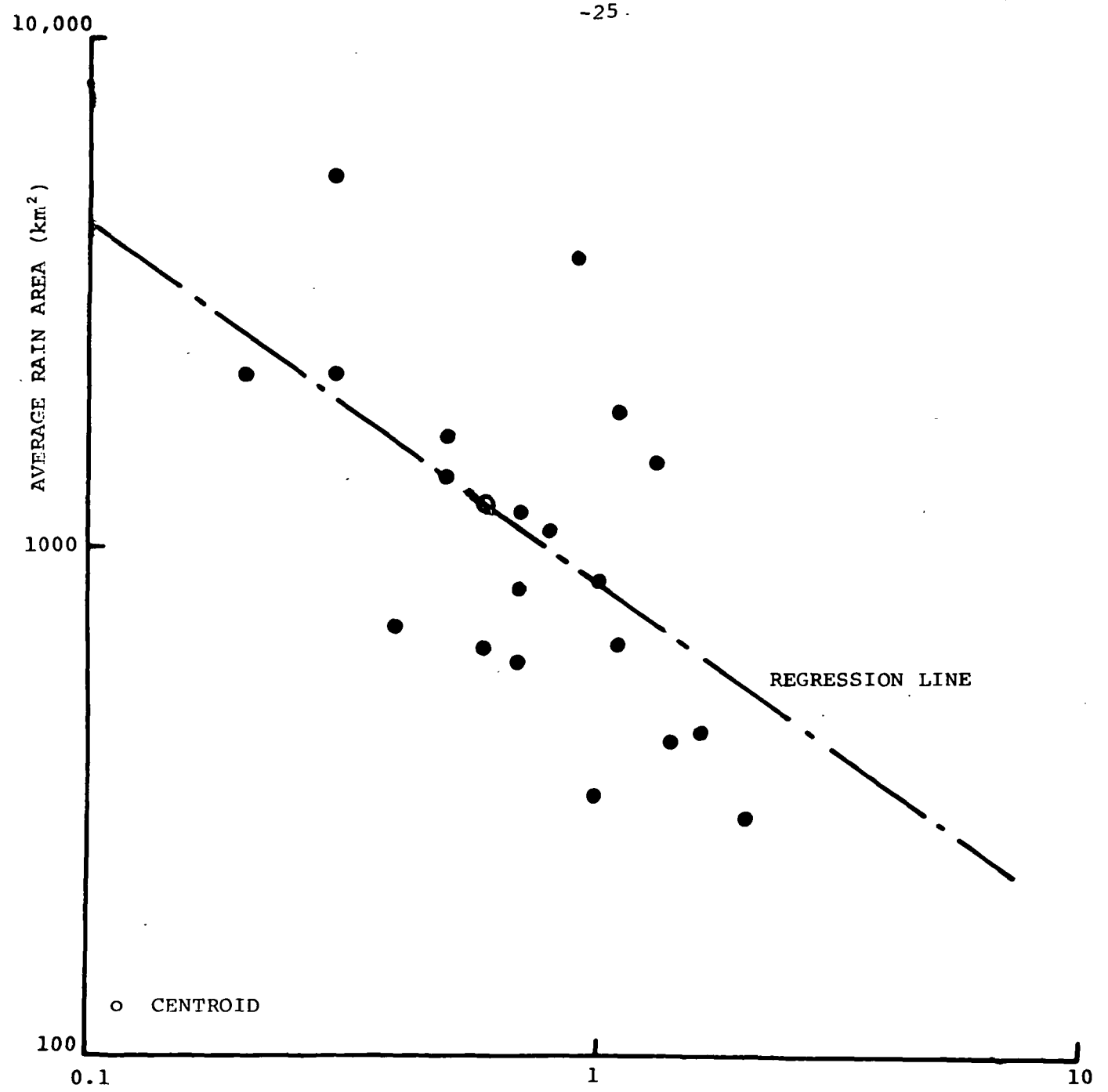
10,000
1000
100
AVERAGE RAIN AREA (km²)
REGRESSION LINE
o CENTROID
0.1
1
10
AVERAGE RAIN RATE (mm/h)

FIGURE 8.

fit relationship. The result is:

$$S_D = 882\ R^{-0.68} \tag{10}$$

where S_D is the debris area for rain rate, R, or

$$W_D = 29.7\,R^{-0.34} \tag{11}$$

where W_D is the length scale for the debris. As before, the shape is not well defined and the relationship between the areas of influence for debris in the vicinity of a point and a line is calculated as for cells:

$$P_D(r \geq R) = (1 + \frac{D}{W_D}) P_D(r \geq R) \tag{12}$$

In the debris, the rain extent may exceed the path length. The path length used in the calculation of the rain rate for a specified path integrated rain rate is either the physical path length or the debris scale length, whichever is smaller. For a long path:

$$R = I/W_D = IR^{0.34}/29.7 \qquad \text{(mm/h)} \tag{13}$$

therefore $R = I^{1.52}/170$ (mm/h)

and $W_D = I/R = 170I^{-.52}$ (Km) (14)

The model for the calculation of the probability that a path integrated rain rate, I, is exceeded may be summarized as

$$W_D = 170\ I^{-0.52} \tag{15}$$

$$W_D' = \text{Minimum } (W_D, D) \tag{16}$$

$$R'' = I/W_D' \tag{17}$$

$$L_D = 29.7(R'')^{-0.34} \tag{18}$$

$$P_D(i \geq I) = (1 + \frac{D}{L_D})\,\eta\,(\frac{\ell n\ R'' - \ell n R_D}{\sigma_D}) \tag{19}$$

$$W_C = \sqrt{5} = 2.24 \tag{20}$$

$$L_C = \text{Minimum } (W_C, D) \tag{21}$$

$$R' = CI/L_C \tag{22}$$

$$C = \frac{1 + 0.7(D - W_C)}{1 + (D - W_C)};\ (D - W_C) > 0;\ C = 1 \text{ otherwise} \tag{23}$$

$$P_C(i \geq I) = (1 + D/W_C)e^{-R'/R_C} \tag{24}$$

The two-component model employs the parameters P_C, R_C, P_D, R_D and σ_D found by fitting the model distribution function

to the empirical distribution function for a rain climate region, the spatial scale parameter W_c and the coefficient of the relationship $W_D = 29.7R^{-0.34}$ deduced from the Kansas radar observations. The distribution function parameters were allowed to change from one climate region to the next but the scale parameters were assumed to apply universally in all climate regions. The rational for the universality of the scale parameters is the similarity in scale of the dynamical processes responsible for the production of rain.

The Two-Component model (2-C Model) was tested by comparison with path average rain rate measurements made in England (Rain Climate - C, Jones and Sims 1978), W. Germany (C, Valentin 1977), Florida (E, Jones and Sims 1978), New Jersey (D2, Freeny and Grabbe 1969) and Illinois (D2, Jones and Sims 1978). The path average observations were obtained in 3 different rain climate regions and each region was different from the rain climate in the high plains of the United States (D1). The measured data were available as path average reduction factors $r = I/RD$ (Crane 1980). The results of the modeled vs. measured path average reduction factors are presented for two path lengths in Figures 9a and 9b. The results show agreement within the apparent statistical uncertainty of the observations. The agreement between the measurements and the Two-Component model predictions justified the use of the universal scale parameter assumption for at least application

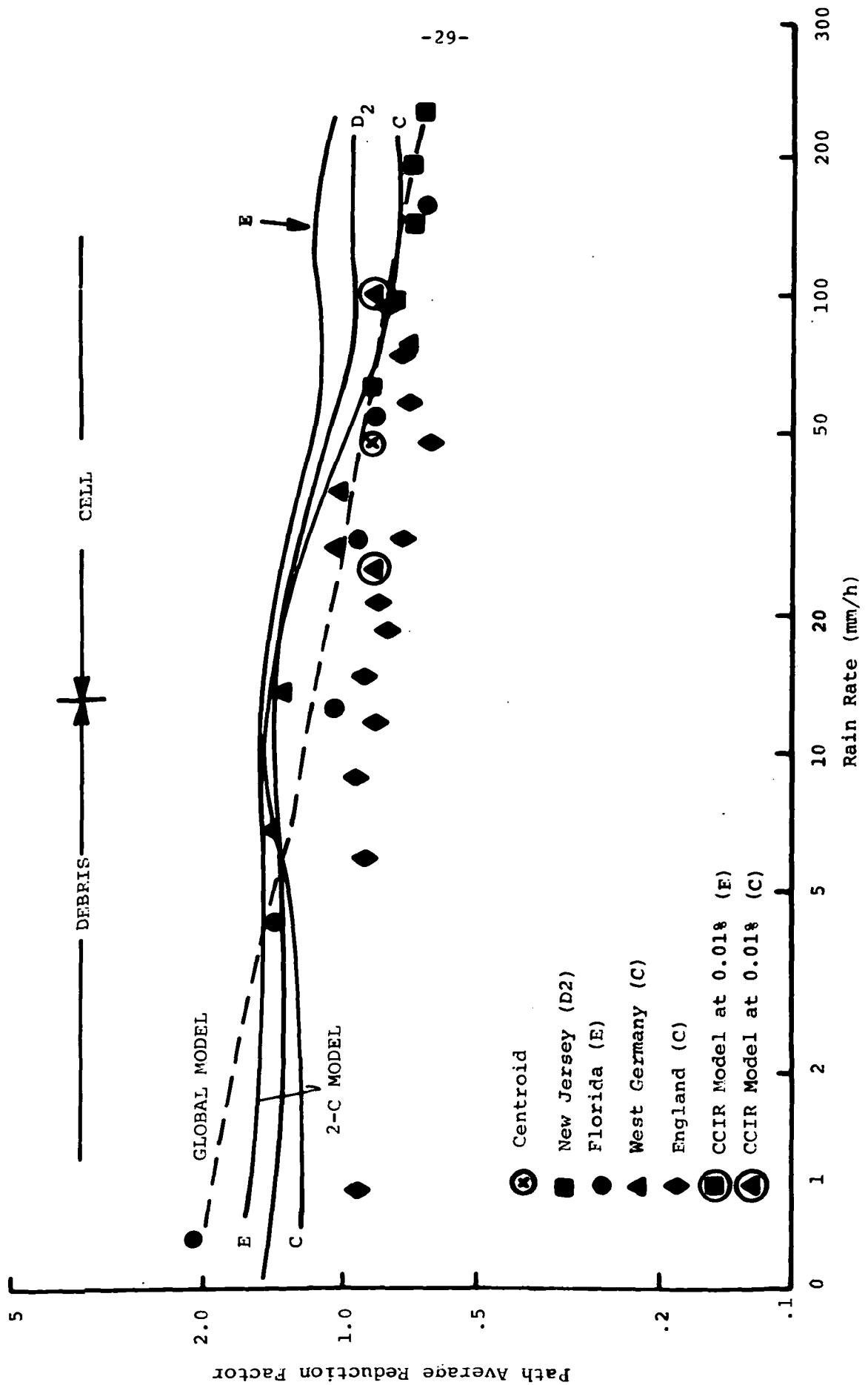
DEBRIS
CELL
GLOBAL MODEL
2-C MODEL
E
C
E
D_2
C
Centroid
New Jersey (D2)
Florida (E)
West Germany (C)
England (C)
CCIR Model at 0.01% (E)
CCIR Model at 0.01% (C)
Path Average Reduction Factor
5
2.0
1.0
.5
.2
.1
0
1
2
5
10
20
50
100
200
300
Rain Rate (mm/h)

FIGURE 9a.

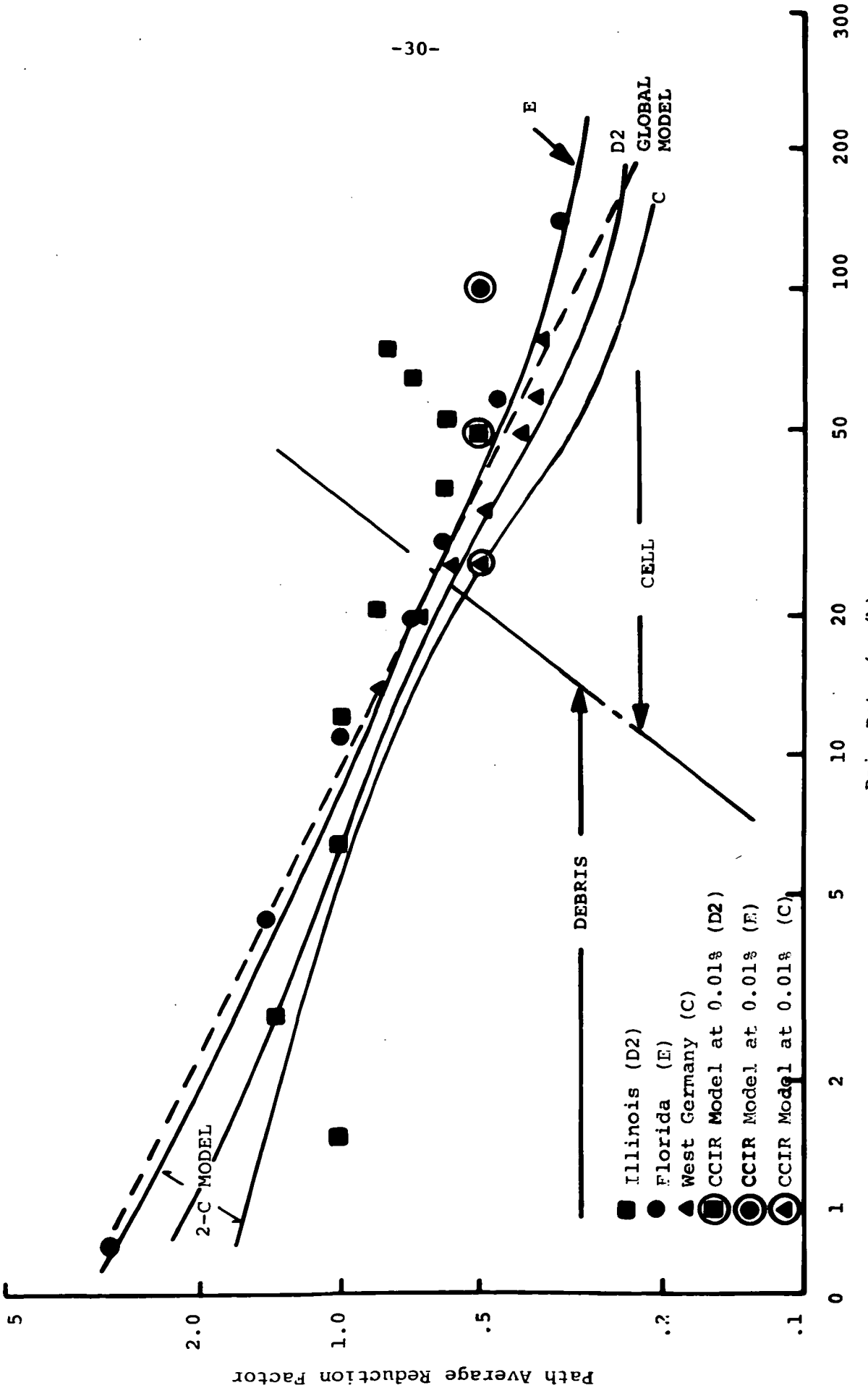
Path Average Reduction Factor
5
2.0
1.0
.5
.2
.1
0
1
2
5
10
20
50
100
200
300
Rain Rate (mm/h)
2-C MODEL
DEBRIS
CELL
E
D2
GLOBAL MODEL
C
Illinois (D2)
Florida (E)
West Germany (C)
CCIR Model at 0.01% (D2)
CCIR Model at 0.01% (E)
CCIR Model at 0.01% (C)

FIGURE 9b.

in temperate climate regions.

2.3 Attenuation on a Terrestrial Path

The attenuation on a terrestrial path is given by

$$a = \int_0^D k[r(\ell)]^{\alpha} d\alpha \tag{25}$$

where a is the attenuation (dB), k, α are coefficients in the relationship, $\gamma = kR^{\alpha}$, and γ is specific attenuation (dB/Km). As for path integrated rain rate, the attenuation within a volume cell is approximated by

$$A \simeq \frac{\gamma W_c}{C_a} = \frac{k}{C_a} R^{\alpha} W_c \tag{26}$$

where A is attenuation (dB) and

$$C_a = C \tag{27}$$

where C_a is the adjustment factor needed to estimate the additional attenuation outside the volume cell. It is noted that the equation (27) for C_a neglects the non-linearity in the relationship between specific attenuation and rain rate. The effect of the non-linearity is small in comparison with the expected year-to-year variations in the observed attenuation or rain rate values at specified probabilities of occurrence. For a Gaussian volume cell profile, the error in calculating

attenuation caused by assuming the C_a vs. C relationship in equation (27) in -3.5% for α = 1.3 and +4.5% for α = 0.75. The error is therefore less than 5% for the entire range of values of α for calculations at frequencies between 1 and 100 GHz (CCIR 1982a). By way of contrast, the year-to-year variability for measured attenuation values at probability values between 0.1 and 0.01% of the year is in excess of 20% (Crane 1980).

The two-component model calculates the probability of exceeding a specified attenuation value after first estimating the rain rate in a volume cell or in the debris region required to produce that value or a higher value of attenuation. For a volume cell,

$$R' = \left(\frac{CA}{kL_c}\right)^{1/\alpha} \quad \text{(mm/h)} \tag{28}$$

and

$$P_c(a \geq A) = (1 + D/W_c)e^{-R'/R_c} \quad \text{(percent)} \tag{29}$$

Similarly, neglecting the effect of the non-linearity on the relationship between average specific attenuation and average rain rate within the debris region,

$$R = \left(\frac{A}{kW_D}\right)^{1/\alpha} = \left(\frac{A}{29.7k}\right)^{1/\alpha} R^{0.34/\alpha} \quad \text{(mm/h)} \tag{30}$$

Therefore,

$$R = \left(\frac{A}{29.7k}\right)^{1/(\alpha-.34)} \quad \text{(mm/h)} \tag{31}$$

and

$$W_D = 29.7^{(\alpha/\alpha-.34)}\ k^{\{.34/(\alpha-.34)\}}\ A^{\{.34/(\alpha-.34)\}} \quad \text{(Km)} \tag{32}$$

then

$$W_D' = \text{Minimum } (W_D, D) \quad \text{(Km)} \tag{33}$$

$$R'' = (A/kW_D')^{1/\alpha} \quad \text{(mm/h)} \tag{34}$$

$$L_D = 29.7\ R''^{-0.34} \quad \text{(Km)} \tag{35}$$

and

$$P_D(a \geq A) = (1 + D/L_D)\ \eta\ \left(\frac{\ell n R'' - \ell n R_D}{\sigma_D}\right) \quad \text{(percent)} \tag{36}$$

Finally,

$$P(a \geq A) = P_C(a \geq A) + P_D(a \geq A) \quad \text{(percent)} \tag{37}$$

is the desired probability that the attenuation value A is exceeded.

2.4 Attenuation on an Earth-Space Path

Earth-space paths traverse attenuating regions of liquid

drops - rain - and regions of ice and snow. The ice and snow contribute little to the attenuation and may be neglected. The region with rain produces the significant attenuation. The physical extent of the attenuating region must be estimated before the volume cell and debris contributions can be calculated. In contrast to the terrestrial path case, the horizontal projection of the rain region is not defined by the physical location of the antennas but is defined by the expected height to which the rain extends.

The height of the rain region depends upon the dynamical and physical processes at work in a storm. Some variation in the height is to be expected, especially in the northern temperate regions where rain or snow may occur at the ground often within the same storm. The rain rate distributions are assumed to represent only periods with rain on the ground and, therefore, a rain region exists above the ground in all rain climate zones.

Rain usually extends from the ground to a height just below the height of the 0°C isotherm in regions of debris. Radar observations of debris are characterized by a bright band or melting region. The reflectivity values generally vary little on average below the melting region and therefore, the specific attenuation can be assumed to be constant from the surface to the base of the bright band in rain debris (neglecting the variation of specific attenuation with the physical temperature of the raindrop). Radar observations reveal this behavior in the tropical Atlantic (Houze 1981) in the eastern United

States (Goldhirsh and Katz 1979) in England (Hall and Goddard 1978), and Japan (Furuhama et al. 1980). Measurements in wintertime, widespread storms, have on occassion, revealed the existance of extensive low level regions of raindrop growth which should effect the average specific attenuation profiles in the debris regions (Cunningham 1952). The warm rain process was initially developed to explain the occurrence of rain showers in the tropics which do not form high enough to reach the 0°C isotherm (Mason 1971).

A wide range of seasonal and storm-to-storm variation can be expected in the height of the rain region in debris. For the estimation of annual attenuation statistics, a model must integrate over these effects or use an effective average height of the rain region which compensates for the variation. The Global model (Crane 1980) employed the natural correlation between wintertime, widespread storms and low rain region heights and intense summertime convection and higher heights do postulate a variation of effective height with the probability of occurrence of specified or higher surface point rain rate values.

The Global model rain height curves are presented in Figure 10. They were constructed using observations of the 0°C isotherm height during periods with precipitation and during periods of excessive precipitation obtained from an analysis of radiosound data, rain occurrence data, and excessive precipitation data for seven spatially separated sites in the United

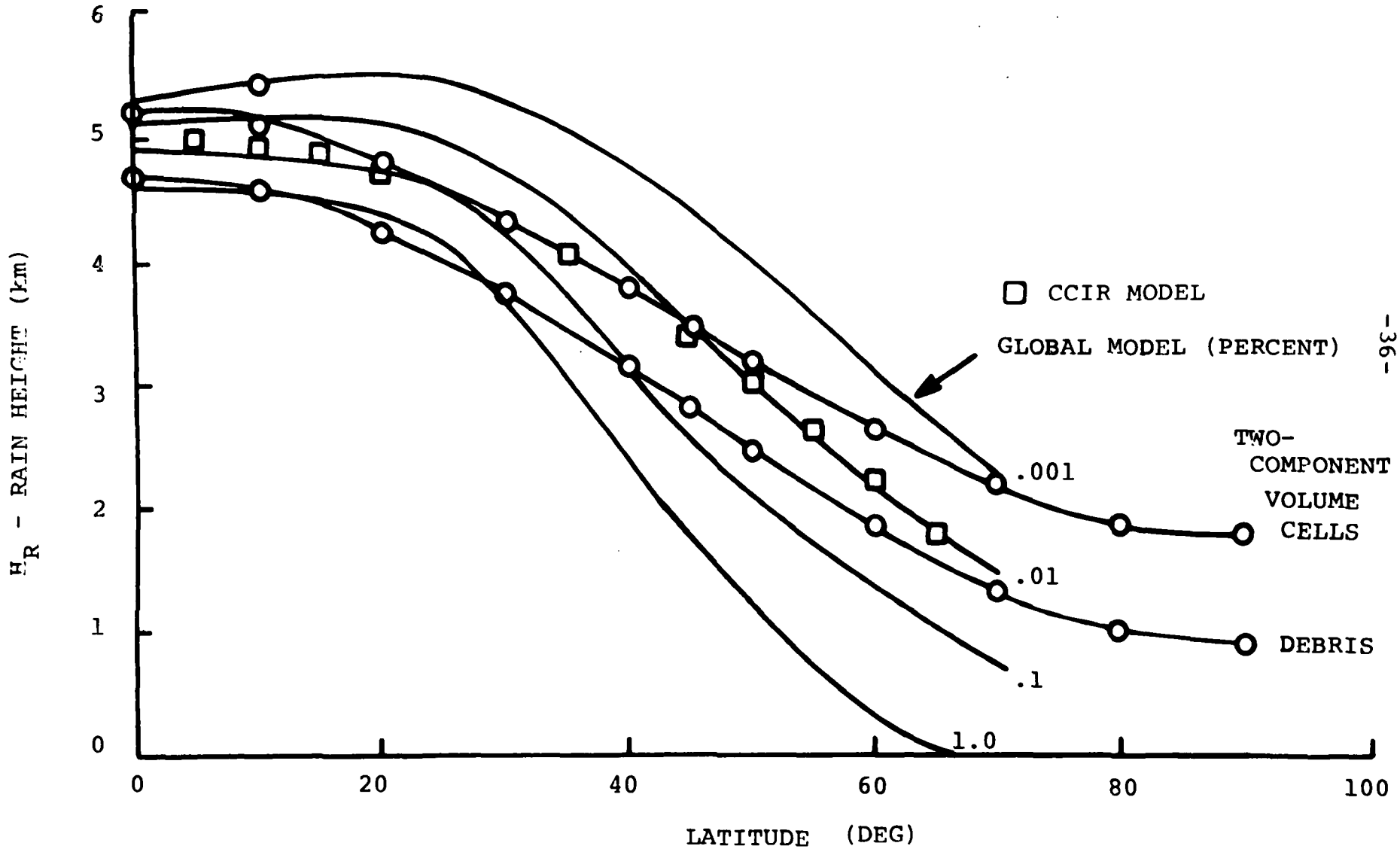
6
5
4
3
2
1
0
H_R - RAIN HEIGHT (km)
0
20
40
60
80
100
LATITUDE (DEG)
CCIR MODEL
GLOBAL MODEL (PERCENT)
.001
.01
.1
1.0
TWO-
COMPONENT
VOLUME
CELLS
DEBRIS

FIGURE 10.

States (Crane 1980). The data were extrapolated globally using the observed latitudinal variation of zonally (longitudinal) averaged temperature profiles. The extrapolations to latitudes higher than 50° were done by selecting summertime data. The 1 percent curve corresponded to the zonally and seasonally averaged 0°C isotherm height (not correlated with precipitation). The 0.001 percent curve corresponded to the 0°C isotherm heights on days with excessive precipitation events (highest 5 minute averaged rain rate each year).

The Two-Component model does not employ the correlation between surface rain rate and rain rate height assumed by the Global model [and by the recently proposed CCIR model, CCIR, (1982b)]. It uses an average rain height for debris of all rain rates and an average rain height for rain in volume cells. Dynamical reasoning suggests that the more intense volume cells will be associated with the updraft regions of a storm which lift liquid particles to higher heights than in the surrounding debris. The observation that the highest rain rate regions in a storm are in the volume cells also argues for a higher volume-cell-rain height than the debris-rain height.

Figure 10 presents the simple latitude variation assumed for the volume cells and the debris. The equations for this dependence are:

$$H_C = 3.1 - 1.7 \sin[2(\Lambda - 45°)] \qquad (38)$$

$$H_D = 2.8 - 1.9 \sin[2(\Lambda - 45°)] \quad (39)$$

where H_c, H_D are the volume cell and debris rain heights respectively (km) and Λ is latitude (deg). For reference, the CCIR model for rain height proposed by Fedi (1981) is also included in this figure.

The simplest sinusoidal variation was assumed to represent the latitude dependence. The debris curve was adjusted to represent the average 0°C isotherm height at low latitudes and the summer time height at high latitudes. The volume cell curve was adjusted to lie above the debris curve with a difference between the two heights roughly equal to the difference between the heights of the 0°C and -5°C isotherms.

The rain heights H_c and H_D define the vertical extent of the rain region. The horizontal extent may be calculated geometrically when the elevation angle to the satellite is given. Two horizontal distances along the earth's surface result, one for volume cells, the other for the debris:

$$D = \frac{(H - H_o)[2 - 2(H - H_o)/8500]}{\tan\theta + \sqrt{\tan^2\theta + (H - H_o)/8500}} \quad \text{(km)} \quad (40)$$

where $D = D_c$, D_D are calculated for $H = H_c$, H_D, respectively, θ is elevation angle, H_o is the height of the earth terminal and an effective earth's radius of 8500 km is assumed.

The expression for the effective debris and volume cell distances D_D and D_c is valid for all elevation angles. It reduces to the familiar $D = (H - H_o)/\tan\theta$ at high elevation angles.

The attenuation values used in the calculation of the probabilities ($P_C(a \geq A_S)$ and $P_D(a \geq A_S,)$ must be reduced to the attenuation along a horizontal path,

$$A = A_S \cos \Theta \tag{41}$$

where A_S is the slant path attenuation and A is the reduced attenuation.

The reduced attenuation value was obtained using an assumed constant specific attenuation from the surface to the rain height. The reduced attenuation value and the effective distances are used in equations (28) through (37) to calculate the desired probability values. Note that although the reduced attenuation values are used in equations (28) and (30) through (34), the resultant probabilities given by equation (29), (36) and (37) are for the full slant path attenuation, As.

3. COMPARISON BETWEEN PREDICTED AND MEASURED ATTENUATION VALUES

The Two-Component model provides a prediction of the attenuation statistics for either a terrestrial or an earth-satellite propagation path. The model is global in nature, proposed for application anywhere, and does not require rain gauge or radar statistics from a location for application at that location. Being global in nature, the model will produce only one set of attenuation statistics for a path of a specified length and frequency located anywhere within a rain climate zone. Observations show that local variations are to be expected within a rain climate zone and perhaps between one side and another of a hill within the same town.

The Global model (Crane 1980) included a set of bounds to be used with the prediction models to describe the expected location-to-location variation within a region or the expected year-to-year variation for a single path. A new variation model is not proposed but the expected variations predicted by the Global model are summarized for consideration when comparing measurements and predictions. For a terrestrial path, the expected rms deviation between model prediction and measurements was estimated to be 29 percent at .1 to .01 percent of the year and 36 percent at 1 and 0.001 percent of the year. For earth-satellite paths, the expected deviations ranged from 32 percent at .1 and 0.01 percent of the year to 39 percent at 1 and 0.001 percent of the year.

The Two-Component model was tested against observations using the procedure proposed by the CCIR (1982a). A test variable, ν, was calculated where

$$\nu = \ell n(A_{measured}/A_{model}) \qquad (42)$$

and the $A_{measured}$ and A_{model} values are equiprobable measured and modeled attenuations. The test variable was calculated at a set of preselected percentages of the year spaced by a ratio of 1.78 (i.e. at .0178, .0316, .052, .1, etc.). The mean and standard deviation of ν was calculated as well as the rms value of ν (the deviation). The prediction method yielding the smallest rms deviation would be judged the method best matching the observations.

The comparison procedure recommended by the CCIR specified that $\nu = 0$ if the measured and modeled attenuation values were within 1 dB. That recommendation was not followed for most of the comparisons presented in this section. Sample calculations showed that the adoption of this CCIR recommendation would have made only a slight difference in the final results.

The model was also tested by calculating the rms deviations in, ξ, the logarithms of the ratios of measured to modeled cumulative probability values at specified attenuation levels. The attenuation values chosen were 1, 2, 3, 5, 7, 10, 15, 20, 25 and 30 dB. The statistics for both the attenuation deviations, ν, and probability

deviation calculations, ξ, were reported as percent deviations,

$$d = (e^{+x} - 1) \cdot 100 \qquad (43)$$

where d is the percent deviation and x is the statistic such as the mean, standard deviation, or rms deviation of ν or ξ.

3.1 Terrestrial Path Observations

The data base employed for the evaluation of the model predictions for terrestrial paths was compiled by Fedi (1981) as a by product of the EUROCOP-COST 25/4 Project (Fedi 1979). Empirical distribution functions were prepared to represent the probabilities that specified attenuation values were exceeded on each of 29 propagation paths in Western Europe, 3 paths in the United States, and 3 paths in Japan. Data from an additional path in Brazzaville, Congo (Moupfouma 1981) were added to the sample to extend the geographical coverage. One or more years of data were available for each path. As reported, only attenuation values in the 0.001 to 0.1 percent of the year range were available.

The mean, standard deviation, and rms deviation values were calculated for ν and ξ for each of the paths and for all the paths. Figure 11 displays sample observations and predictions for two terrestrial paths for a frequency of

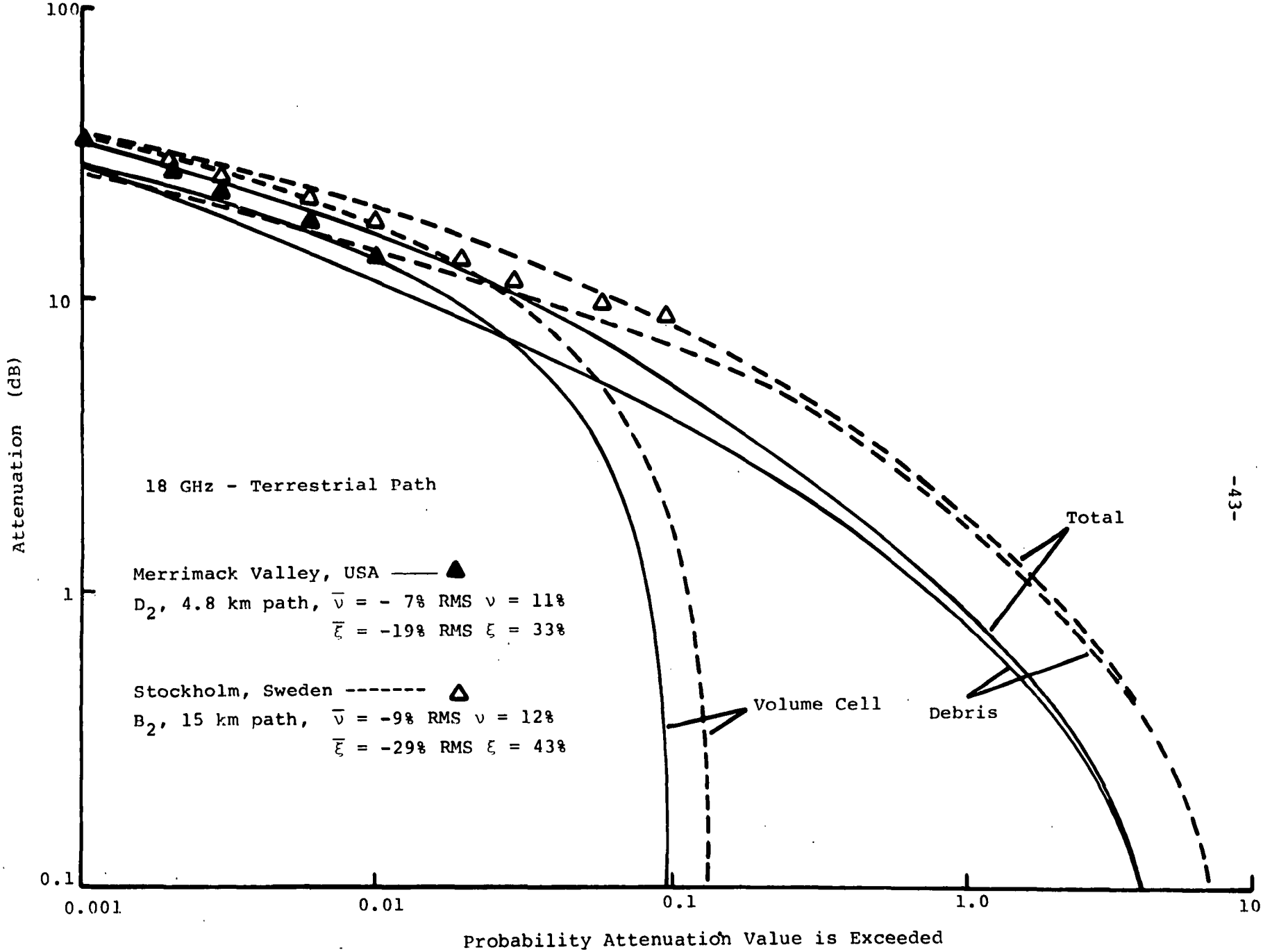
100
10
1
0.1
Attenuation (dB)
18 GHz - Terrestrial Path
Merrimack Valley, USA ——
D_2, 4.8 km path, $\overline{\nu}$ = - 7% RMS ν = 11%
$\overline{\xi}$ = -19% RMS ξ = 33%
Stockholm, Sweden -------
B_2, 15 km path, $\overline{\nu}$ = -9% RMS ν = 12%
$\overline{\xi}$ = -29% RMS ξ = 43%
Total
Volume Cell
Debris
0.001
0.01
0.1
1.0
10
Probability Attenuation Value is Exceeded

FIGURE 11.

18 GHz. The test statistics are listed in the figure. Figure 12 displays the individual path values for the mean (bias) and rms deviation of ν plotted as a function of carrier frequency and Figure 13 displays the same data plotted as a function of path length. No obvious dependences on frequency or path length were evident. A significant source of deviation between model prediction and measurement was the difference between the predicted and observed rain rate. Figure 14 displays this source of modeling error. In this figure, the ordinate is $\bar{\nu}$, the average value of ν for a path, and the abscissa is the natural logarithm of the ratio of the measured to modeled rain rate corresponding to 0.01 percent of the year. From this figure, it is evident that the modeling uncertainty is increased by using the rain zone estimates of the rain rate distributions in place of the reported rain rate distributions for each location.

The average model bias, $\bar{\nu}$, for all the paths was -9.8 percent. The average of the $\bar{\nu}$ values for each of the paths was -15.7 percent (centroid location in Figure 14). The difference between the two values arose from the different weights accorded to the individual ν values. Up to 9 attenuation ratio values (ν values) were possible for a single path but many paths had fewer due to dynamic range limitations of the instrumentation.

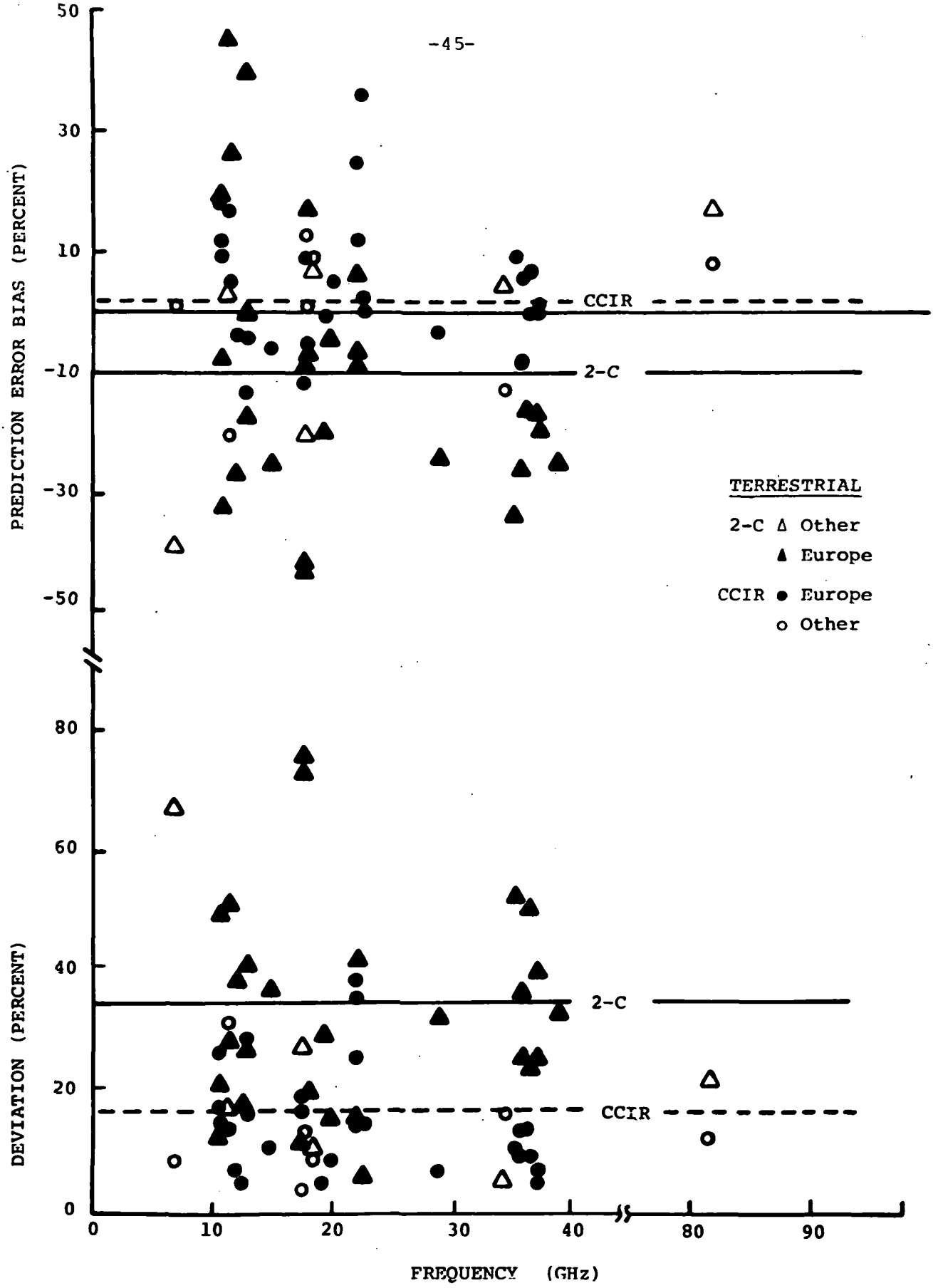
PREDICTION ERROR BIAS (PERCENT)
DEVIATION (PERCENT)
FREQUENCY (GHz)
CCIR
2-C
2-C
CCIR
TERRESTRIAL
2-C Δ Other
▲ Europe
CCIR ● Europe
o Other
50
30
10
-10
-30
-50
80
60
40
20
0
0
10
20
30
40
80
90

FIGURE 12.

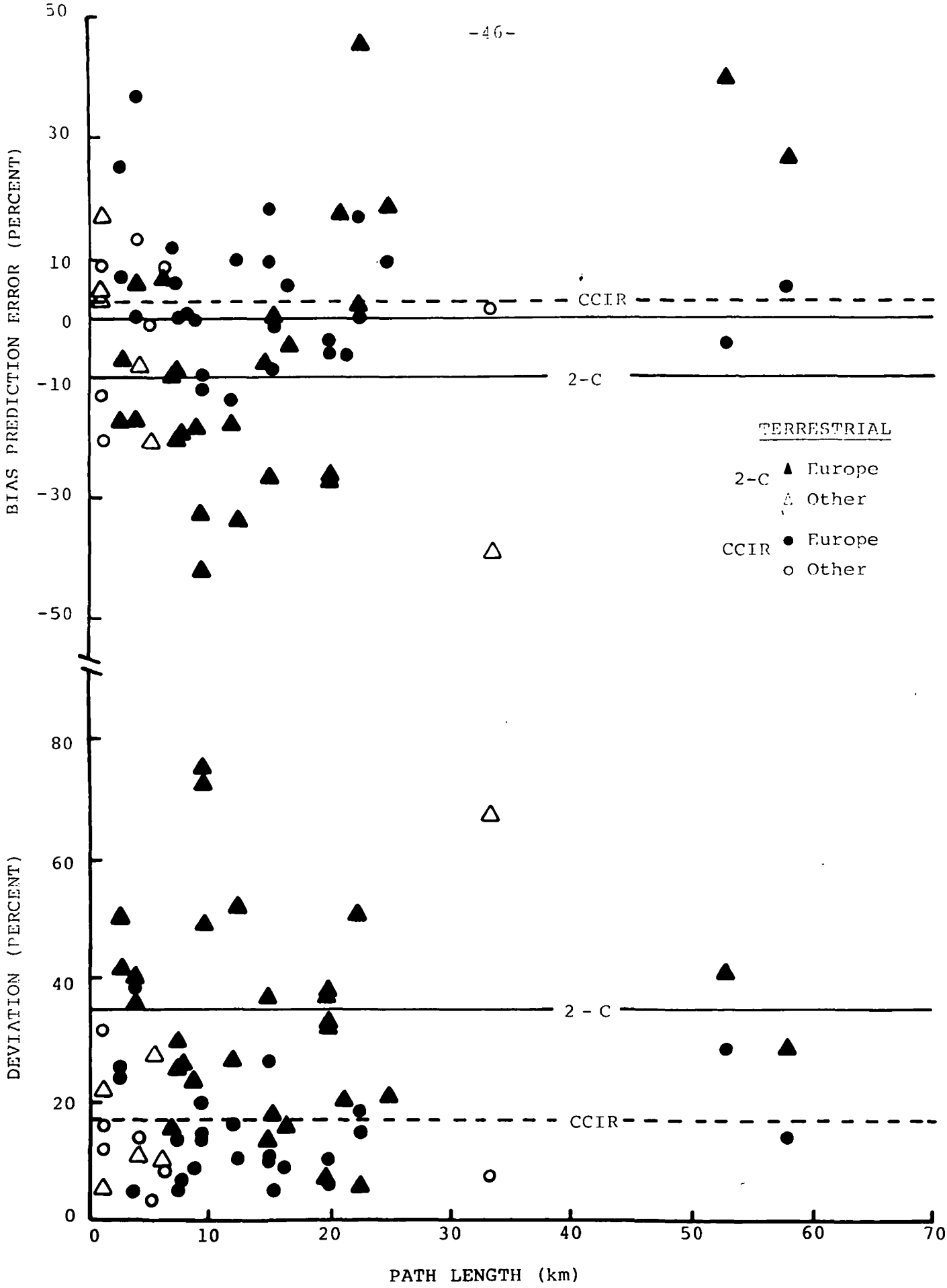
BIAS PREDICTION ERROR (PERCENT)
DEVIATION (PERCENT)
PATH LENGTH (km)
50
30
10
0
-10
-30
-50
80
60
40
20
0
10
20
30
40
50
60
70
CCIR
2-C
2 - C
CCIR
TERRESTRIAL
2-C Europe
Other
CCIR Europe
Other

FIGURE 13.

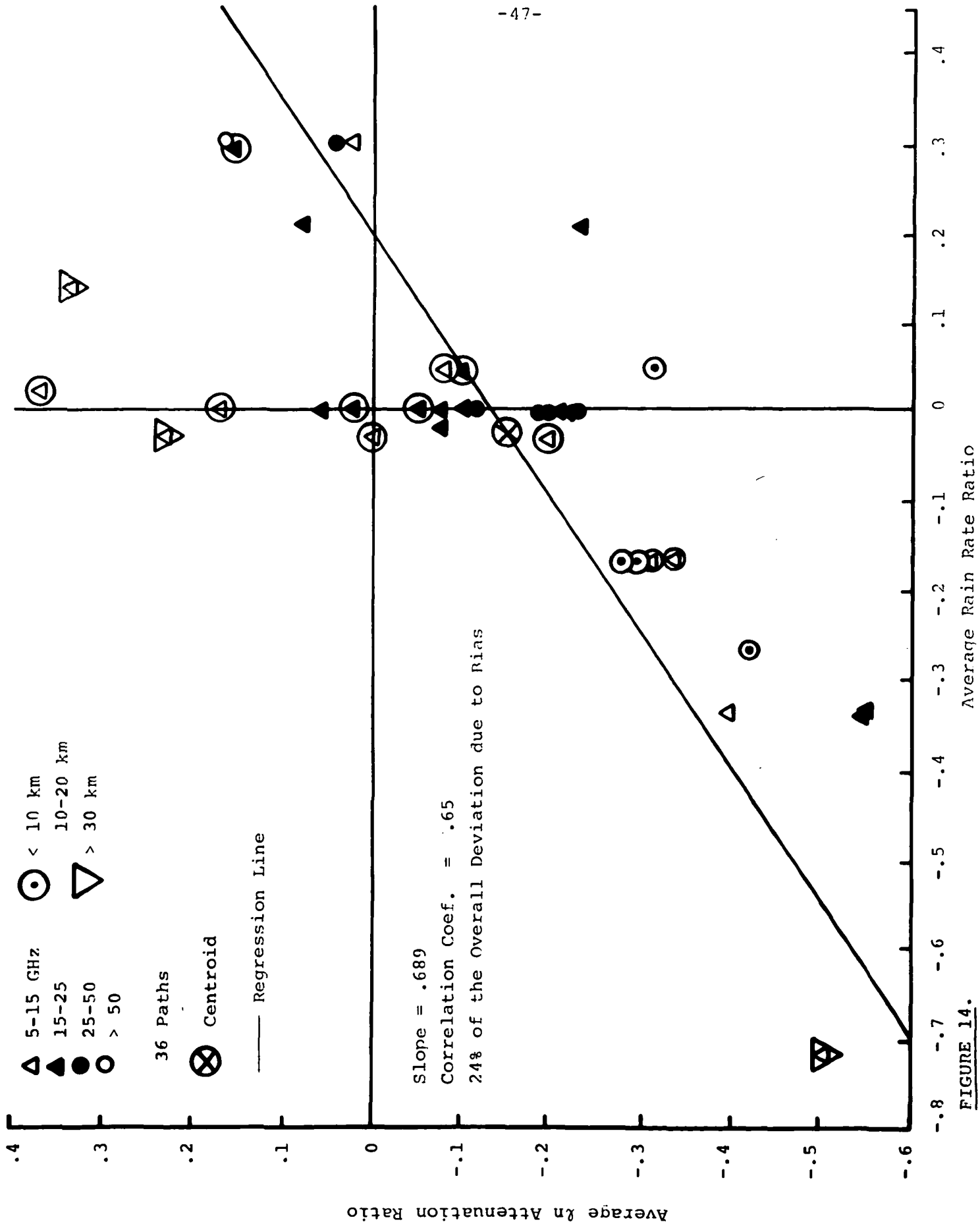
5-15 GHz
15-25
25-50
> 50
< 10 km
10-20 km
> 30 km
36 Paths
Centroid
Regression Line
Slope = .689
Correlation Coef. = .65
24% of the Overall Deviation due to Bias
Average kn Attenuation Ratio
Average Rain Rate Ratio
.4
.3
.2
.1
0
-.1
-.2
-.3
-.4
-.5
-.6
-.8
-.7
-.6
-.5
-.4
-.3
-.2
-.1
0
.1
.2
.3
.4

FIGURE 14.

The standard deviation of ν was 32.7 percent and the rms deviation of ν was 35.2 percent. The expected rms deviation for an error free model caused only by location and yearly variations as predicted by the Global model is 30.8 percent, in close agreement with the test statistic.

The average model bias calculated using probability deviations, $\overline{\xi}$, was -23.2 percent. The standard deviation and rms deviation of ξ were 135 and 145 percent respectively. These variations are significantly higher than those for ν. No model estimates are currently available for the variation in ξ to be expected.

The evaluation of the utility of the Two-Component model was completed by comparing the test statistics for this model with the test statistics for the recently proposed CCIR model (Fedi 1981, CCIR 1982b; see Appendix A for a description of the model). The mean, standard deviation and rms deviation values for ν were 2.4 percent 16.3 percent, and 16.5 percent respectively. The bias, $\overline{\nu}$, and rms deviation values for the individual paths are also plotted in Figures 12 and 13. The Two-Component model (2-C) produced 3.7 times the mean square deviation of the CCIR model. A significant fraction of the increased mean square deviation is due to the use of a regional rain rate distribution in place of the observed distribution as recommended for the CCIR model. However, the two models performed as expected on the basis

of the Global model prediction of variation about the estimated values. When the rain rate distribution is known, the bias should be small and the rms deviation should be 18 percent. The CCIR model produced a bias, $\bar{\nu}$, 2.4 percent and an rms deviation of 16.5 percent.

The CCIR model test statistics for probability deviations were bias, $\bar{\xi}$, equal to 17.7 percent, a standard deviation of 43.6 percent and an rms deviation of 48.8 percent. As for the attenuation deviations, the CCIR model performed better than the Two-Component model.

The CCIR model was developed by adjusting the coefficients to fit western European observations of attenuation exceeded 0.01 percent of the year. An additional comparison between the two models was performed using only the attenuation ratio values at 0.01 percent of the year and the complete recommendations of the CCIR for model comparison ($\nu = 0$ if the attenuation values differ by less than 1 dB). For this comparison data were available for 28 western European paths, 3 for the United States and 3 for Japan. The rms deviations for the western European data were 33.4 percent and 14.3 percent for the Two-Component and CCIR models respectively. For the United States, the rms deviations were 15.7 and 9.8 respectively and for Japan the rms deviations were 0 and 4.2 percent, respectively. Although the number of non-European samples was small, the Two-Component model did better relative to the CCIR model outside Europe than for

Europe. Overall, the rms deviations were 30.3 percent and 13.3 percent for the Two-Component model and CCIR model respectively.

3.2 Earth-Satellite Path Observations

Attenuation observations were assembled from 17 earth-space paths in the United States, 10 in Europe and 20 in Japan for which data were available for a year or more. The data were reported in the CCIR (1982b) at three percentages of the year or by Ippolito et al. (1981). Examples of measured and Two-Component model predicted attenuation distributions for the CTS satellite observations at 11.7 GHz and from the COMSTAR satellite at 28.6 GHz are presented in Figure 15. The observations were all made in rain climate region D2 therefore, the only possible model value differences are due to the variation in elevation angle and rain height. Lin et al. (1980) reported that at higher frequencies, the elevation angle and latitude variations compensate for one another when viewing the same satellite, a result apparent at 0.1 to 1.0 percent of the year at 28.6 GHz. The additional variability evident at 11.7 GHz and at the probability range extremes at 28.6 GHz must be due to local and yearly rain rate differences and, perhaps, the instrumentation.

The test statistics for ν and ξ were calculated for each of the 47 earth-satellite paths. The results for the attenuation ratio statistics were a bias, $\bar{\nu}$, of -10 percent

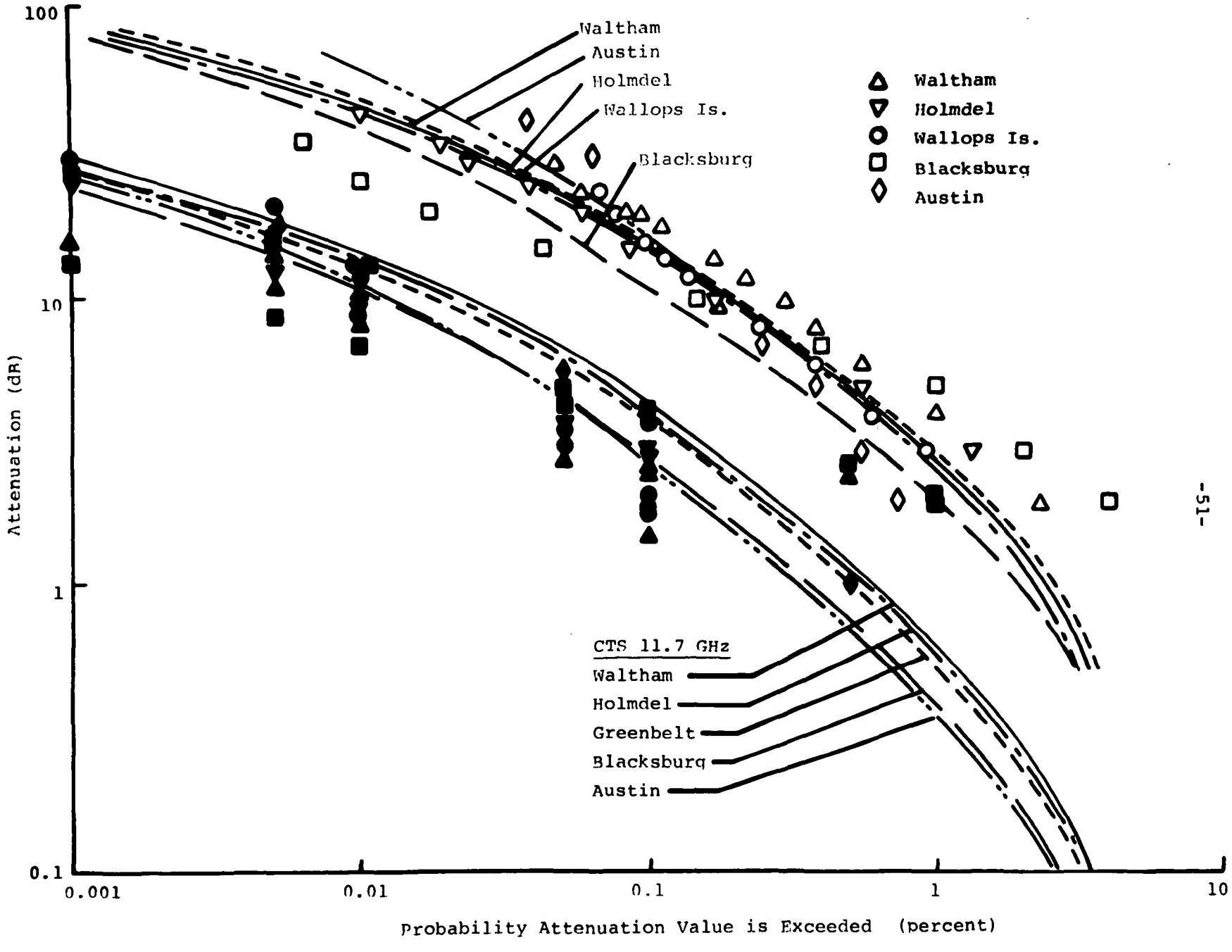
28.6 GHz COMSTAR
100
10
1
0.1
Attenuation (dB)
Waltham
Austin
Holmdel
Wallops Is.
Blacksburg
Waltham
Holmdel
Wallops Is.
Blacksburg
Austin
CTS 11.7 GHz
Waltham
Holmdel
Greenbelt
Blacksburg
Austin
0.001
0.01
0.1
1
10
Probability Attenuation Value is Exceeded (percent)

FIGURE 15.

a standard deviation of 77 percent and an rms deviation of 79 percent. The bias value was nearly identical to the bias value for application of the model to terrestrial paths but the variances were a factor of 3.7 larger, 79 vs. 35 percent rms deviation. The model performance was consistent with expectations in the United States, the rms deviation for ν was 35.9 percent when only the paths in the United States were included, but was poorer than expected for Japan where the observed rms deviation was 116 percent.

The overall probability ratio statistics for the Two-Component model were nearly the same for the slant path and the terrestrial path observations. For the slant path, the bias, $\overline{\xi}$, was -13.7 percent, the standard deviation was 139 percent and the rms deviation was 142 percent.

The attenuation ratio statistics for the individual paths are depicted as a function of frequency in Figure 16 and as a function of latitude (and by implication, elevation angle and path length) in Figure 17. Again, no obvious dependences of the model predictions in frequency or on latitude are evident. The model performs well over the entire 24 to 53° latitude band spanned by the observations. The high variance values appear to be caused by a limited number of paths. One such path, Ogasawara, Japan, produced an rms deviation in ν of 195 percent and in ξ of 948 percent. For this path, at an elevation angle of 43°, latitude of 27° and a frequency of 12.1 GHz, the predicted attenuation to be

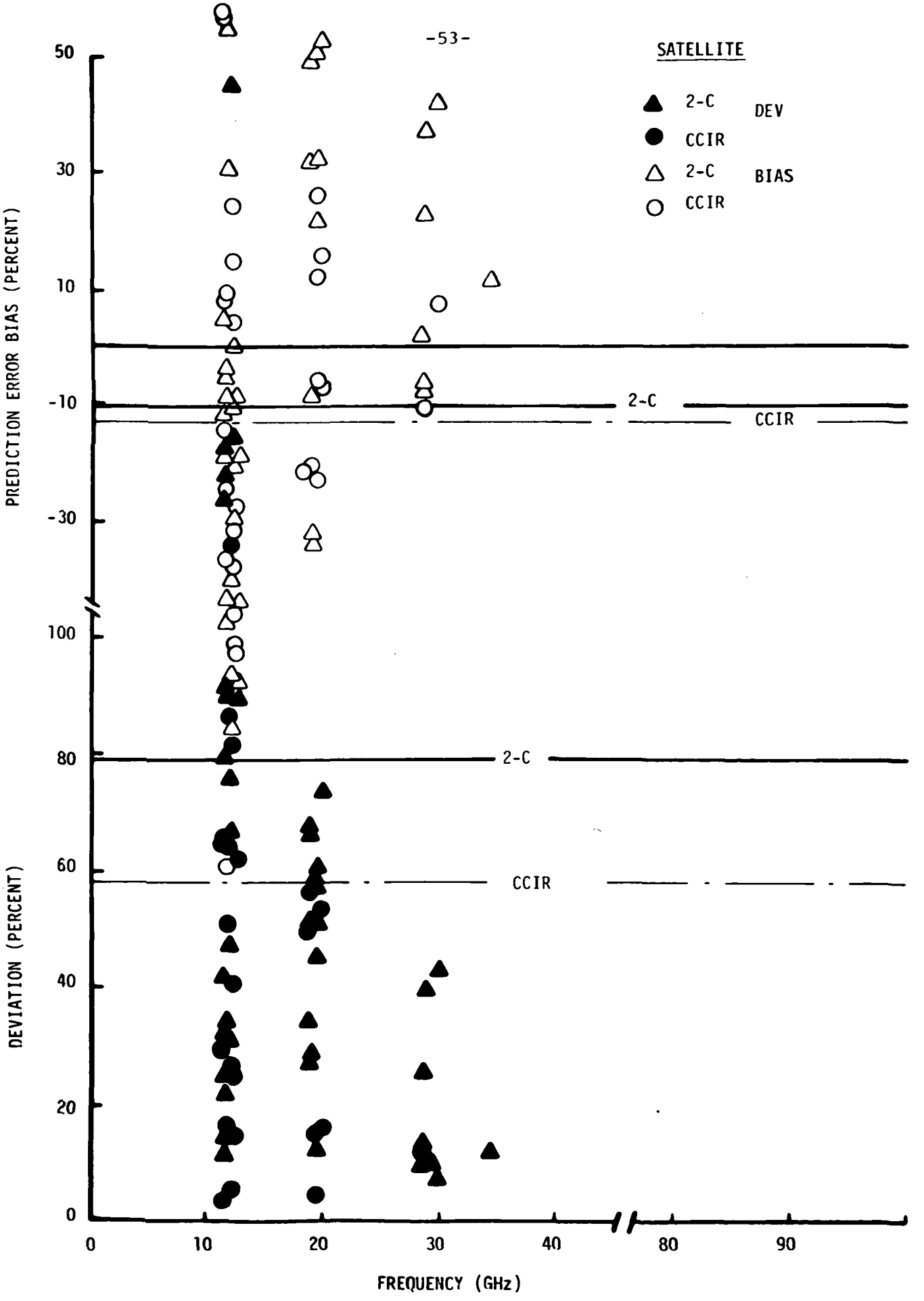
SATELLITE
2-C DEV
CCIR
2-C BIAS
CCIR
PREDICTION ERROR BIAS (PERCENT)
DEVIATION (PERCENT)
50
30
10
-10
-30
100
80
60
40
20
0
2-C
CCIR
2-C
CCIR
0
10
20
30
40
80
90
FREQUENCY (GHz)

FIGURE 16.

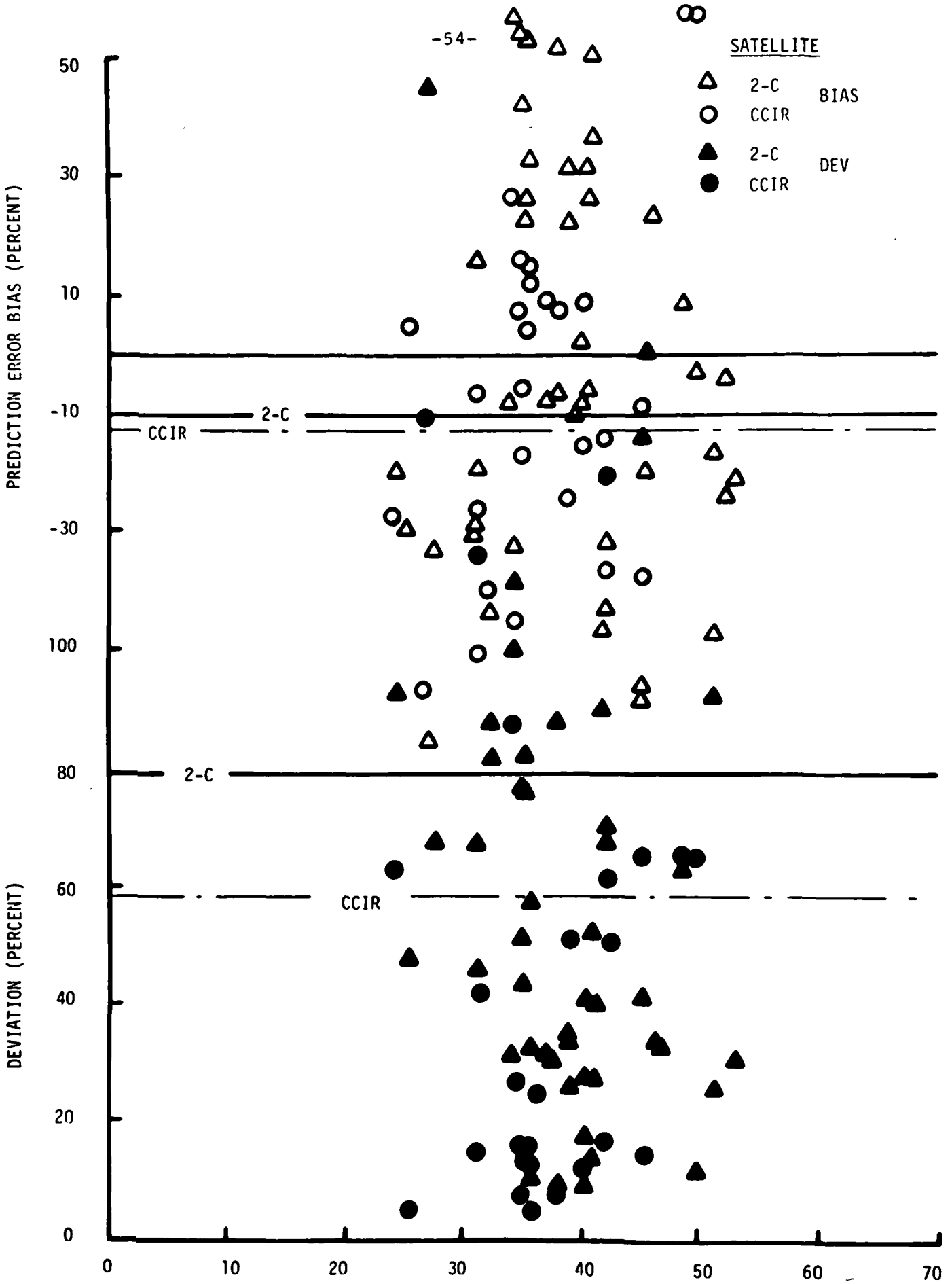
SATELLITE
2-C BIAS
CCIR
2-C DEV
CCIR
PREDICTION ERROR BIAS (PERCENT)
DEVIATION (PERCENT)
50
30
10
-10
-30
100
80
60
40
20
0
2-C
CCIR
2-C
CCIR
0
10
20
30
40
50
60
70
N. LATITUDE (DEG)

FIGURE 17.

exceeded 0.001 percent of the year was 48 dB, the observed value was 11 dB. For comparison, this path also produced large rms deviations from the CCIR model. The rms deviation values for ν and ξ were 139 and 1323 percent respectively. At 0.001 percent of the year, the simplified CCIR model predicted an attenuation of 39 percent. Other paths at similar or lower latitudes did not produce similar large deviations, therefore, the large errors for this path cannot be attributed to the rain height component of the model or, from the large discrepency relative to the CCIR model, in the difference between modeled and measured rain rate distributions.

The simplified CCIR model (Appendix A) was used to provide comparison test statistics for the Two-Component model when applied to earth-satellite paths. The simplified model used an approximation to the rain height curve of the Global model for 0.01 percent of the year (Figure 10) and provided predictions only in the 0.1 to 0.001 percent of the year probability range. Simultaneous rain rate statistics were available only for 31 of the 47 paths. The attenuation ratio statistics, $\overline{\nu}$ and rms deviation of ν were -12.7 and 57.9 percent respectively. The simplified CCIR model did not perform as well relative to the Two-Component model as it did for terrestrial paths. The mean square

deviation was only a factor of 1.6 smaller than the mean square deviation for the Two-Component model even though the measured rain rate statistics were used in applying the CCIR model. The CCIR model probability deviation statistics were also poorer relative to the Two-Component model for slant paths than for terrestrial paths. The observed bias, $\bar{\xi}$, was -2.4 percent but the rms deviation in ξ was 165 percent, larger than the 142 percent for the Two-Component model.

The Two-Component and CCIR models were compared for predictions at 0.01 percent of the year. The two models were nearly identical when tested against data from the United States: 26.2 percent rms deviation in ν for the Two-Component model; 21.4 percent rms deviation for the CCIR model. The Two-Component model performed better in Europe: 44.3 percent rms deviation in ν for the Two-Component model; 84.5 percent rms deviation for the CCIR model. In Japan, the relative performances of the two models were reversed: 76.1 percent rms deviation in ν for the Two-Component model; 36.3 percent for the CCIR model.

3.3 Summary

The two models performed as expected when applied to terrestrial paths. The major difference between the two related to the use of the observed rain rate distribution

(at 0.01 percent of the year) in the CCIR model and the use of the rain climate region distributions in the Two-Component model.

The Two-Component model performed relatively better than the CCIR model when employed for predictions on earth-satellite paths. For data from the United States, the performance of the Two-Component model was as expected but, when employed to provide predictions for Japan the performance was not as good as expected.

4. PREDICTION OF JOINT ATTENUATION STATISTICS

At frequencies above 10 GHz, the reliability of a single earth-satellite communication path is not as high as desired for communication system performance. One way proposed to improve system reliability is to employ space diversity. To evaluate the utility of space diversity systems, models are required to predict the diversity improvement (advantage) or diversity gain to be expected for closely spaced diversity paths. Current models are empirical in nature employing functions fit to diversity gain or advantage observations. The Two-Component model provides an alternative procedure for estimating the joint attenuation statistics for diversity paths with spacings less than about 20 km.

4.1 Joint Statistics Model

The prediction of the probability of exceeding a specified attenuation on a single path was obtained by summing the probabilities that the specified attenuation values were produced by volume cells or by debris. A spatial scale, W_c or W_D was associated with the volume cell or debris. The probability calculation required an estimate of the probability that rain with the appropriate spatial scale occurred along the propagation path. This model was extended to calculate the joint occurrence statistics by

calculating the probability that a volume cell or debris region simultaneously affected both propagation paths. As with the procedure for calculating the required area ratios (Figure 7) for a single path, the exact calculation depends upon the shape of the volume cell or of the debris region. Since no shape information was available, the simplest possible model was chosen. Its application is illustrated in Figure 18.

The simplest model employs the square cell aligned along the propagation path. For earth-satellite paths, the case considered in this paper, the propagation paths are parallel when communication is from each site to the same geostationary satellite. The area occupied by a volume cell or debris region of scale W which affects both paths simultaneously is

$$S_j = W^2 \left(1 - \frac{L \sin\beta}{W}\right) \left(1 + \frac{D - L \cos\beta}{W}\right) \qquad (43)$$

where L is the baseline separation between the diversity sites, β is the orientation angle of the baseline relative to the propagation path, $W = W_c$ or W_D for volume cells or debris respectively and D is the horizontal projection of the path length, D_c or D_D for volume cells or debris respectively.

The probability of the joint occurrence of a specified

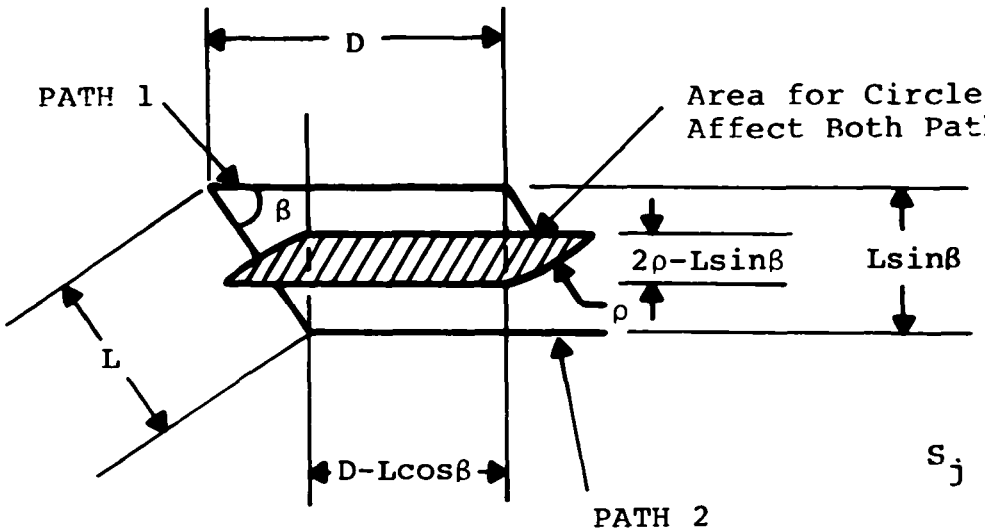

$$S_j = (2\rho - L\sin\beta)(D - L\cos\beta) + \text{End Areas}$$

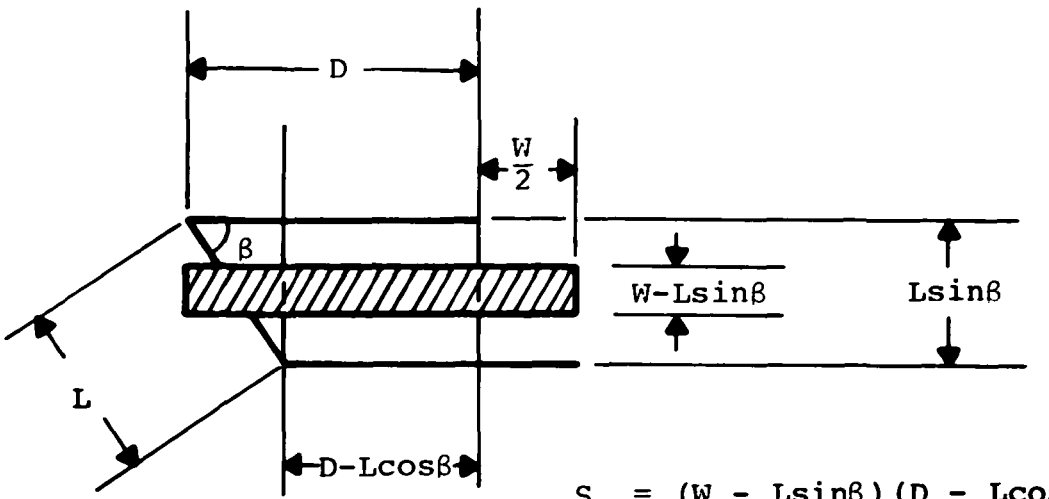

$$S_j = (W - L\sin\beta)(D - L\cos\beta) + W(W - L\sin\beta)$$

$$= W^2\left(1 - \frac{L\sin\beta}{W}\right)\left(1 + \frac{D - L\cos\beta}{W}\right)$$

$$= S_c\left(1 - \frac{L\sin\beta}{W}\right)\left(1 + \frac{D - L\cos\beta}{W}\right)$$

FIGURE 18.

or higher attenuation on both paths simultaneously is given by

$$P_j = \left(1 - \frac{L \sin\beta}{w_D}\right)\left(1 + \frac{D - L\cos\beta}{w_D}\right) P_D(r \geq R'')$$

$$+ \left(1 - \frac{L \sin\beta}{w_c}\right)\left(1 + \frac{D - L\cos\beta}{w_D}\right) P_c(r \geq R')$$

$$+ 0.01\,[P(a \geq A)]^2 \qquad \text{(percent)} \qquad (44)$$

where the R', R" values were obtained in the calculation of $P_c(a \geq A)$ and $P_D(a \geq A)$ respectively and the final term is the square of the single site probability value (adjusted by 0.01 to provide probability values in percent) represents the joint probability for independent events. The multipliers, $\left(1 - \frac{L \sin\beta}{w}\right)$ and $\left(1 + \frac{D - L\cos\beta}{w_D}\right)$ obtain only when positive. If negative, the multiplier is replaced by zero because the baseline is too large for a volume cell or debris region to simultaneously affect both paths.

This model is the simplest possible consistent with the assumptions underlying the Two-Component model which includes the baseline length and orientation and the parameters needed to calculate the single site attenuation statistics. The size of the volume cell was assumed to be constant in the Two-Component model and small, $w_c = 2.24$ km. The same volume cell therefore cannot affect both paths at once if

L sinβ > 2.24 km. Since L sinβ is generally larger than 5 km for diversity application, a diversity gain or improvement is obtained when the volume cells are the dominant cause of the attenuation.

4.2 Comparison with Measurements

In sufficient data were available for a statistical evaluation of the Two-Component model for the estimation of the joint statistics or the values of diversity gain or advantage which can be obtained from the joint statistics. Sample comparisons are presented in Figures 19 through 21 for satellite observations, radar simulations, and radiometer measurements made in the eastern United States and Canada. Figure 19 illustrates the calculation of single and joint site statistics for a low elevation angle path at 11.6 GHz (Towner et al. 1982). The two site independent distribution represents the final term in equation (44) and represents the best possible two site diversity results. The attenuation ratio statistics, $\overline{\nu}$, and the rms deviation in ν were - 2 percent and 6.5 percent respectively for the joint distribution. For this one pair of diversity paths, the Two-Component model exactly predicted the observations. The empirical models reported by Ippolito et al. (1981) consistently predicted better diversity performance for this path.

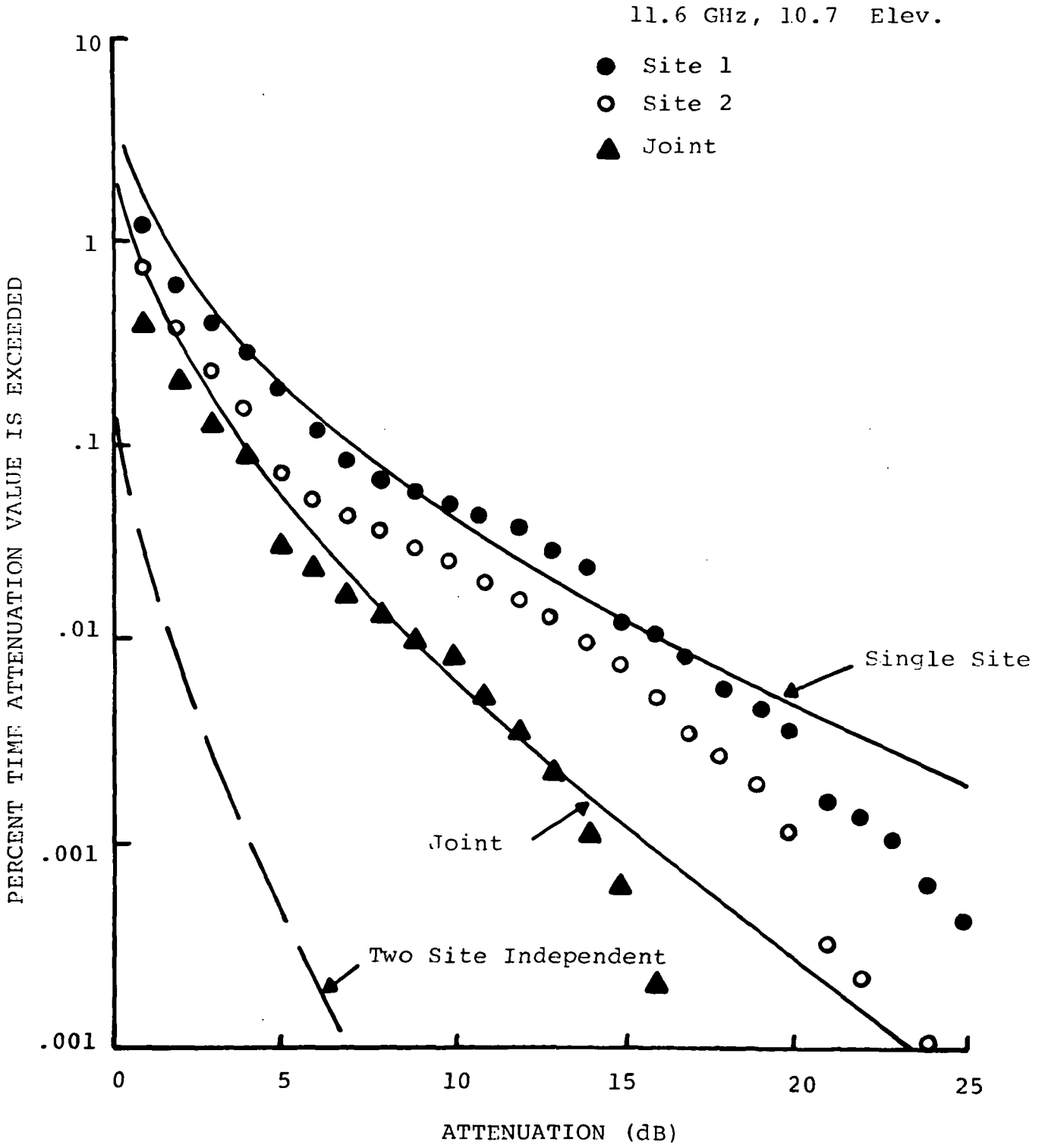
11.6 GHz, 10.7 Elev.
Site 1
Site 2
Joint
10
1
.1
.01
.001
.001
PERCENT TIME ATTENUATION VALUE IS EXCEEDED
Single Site
Joint
Two Site Independent
0
5
10
15
20
25
ATTENUATION (dB)

FIGURE 19.

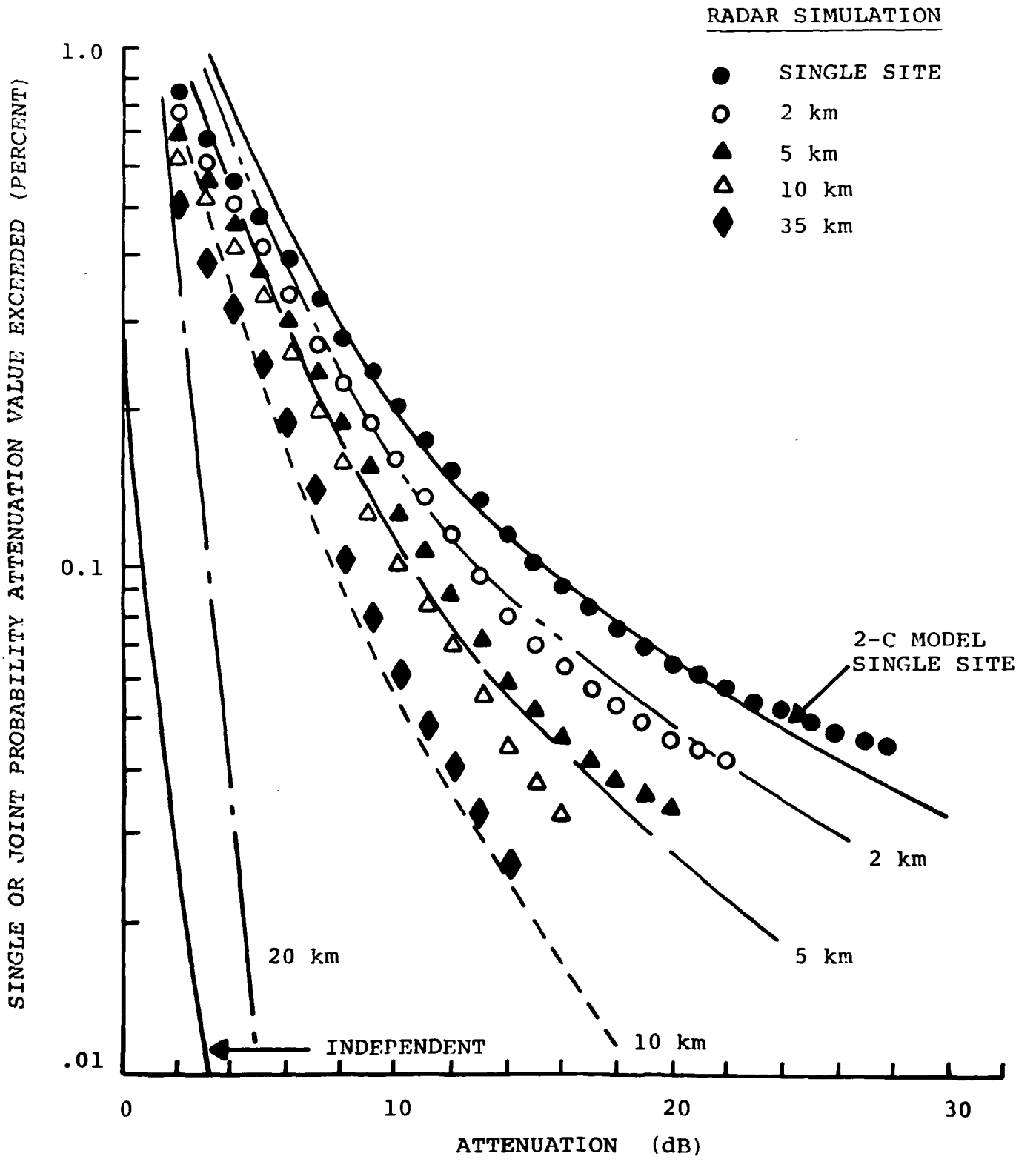
RADAR SIMULATION
SINGLE SITE
2 km
5 km
10 km
35 km
1.0
0.1
.01
SINGLE OR JOINT PROBABILITY ATTENUATION VALUE EXCEEDED (PERCENT)
2-C MODEL
SINGLE SITE
2 km
5 km
10 km
20 km
INDEPENDENT
0
10
20
30
ATTENUATION (dB)

FIGURE 20.

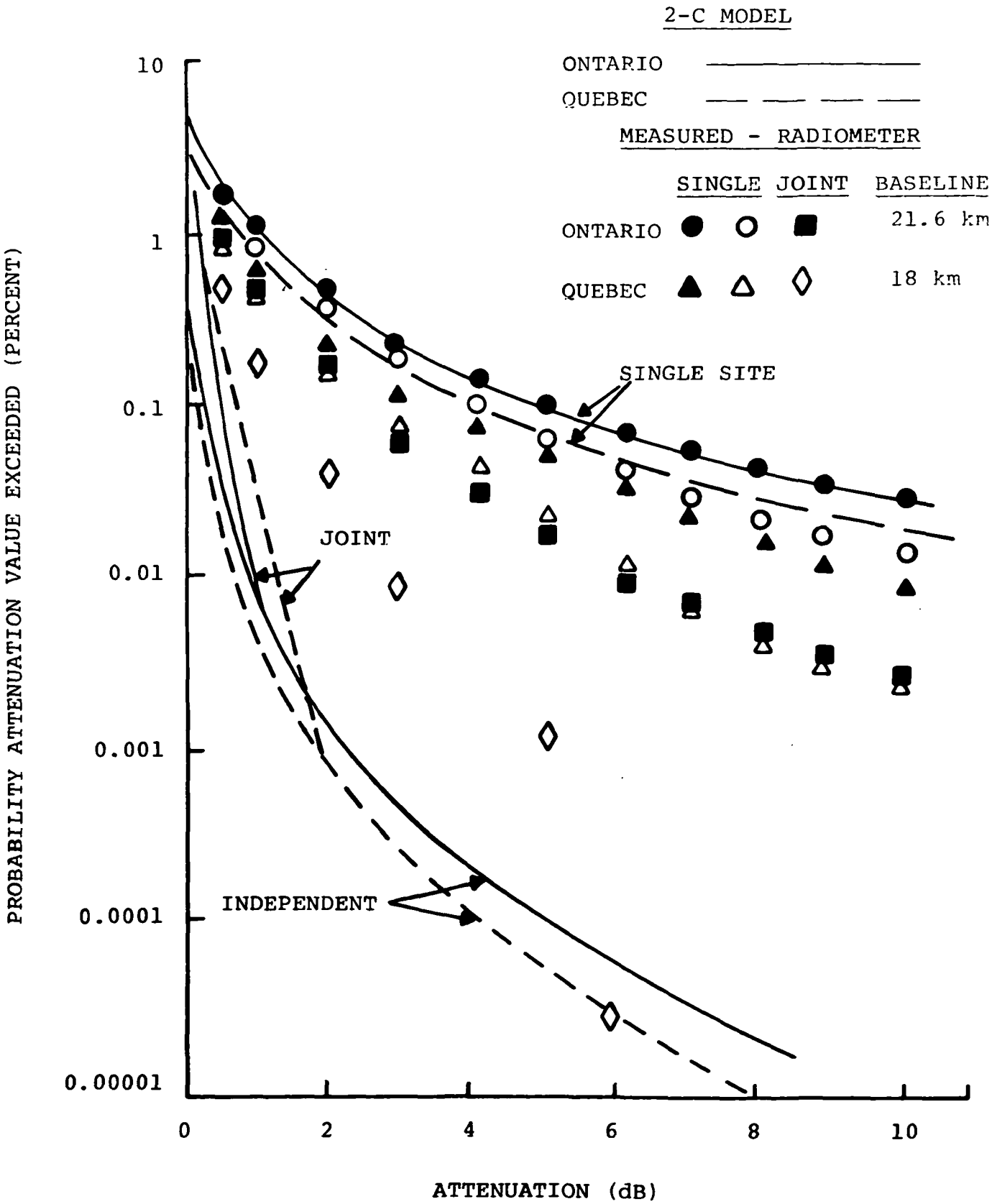
2-C MODEL
ONTARIO
QUEBEC
MEASURED - RADIOMETER
SINGLE JOINT BASELINE
ONTARIO 21.6 km
QUEBEC 18 km
SINGLE SITE
JOINT
INDEPENDENT
PROBABILITY ATTENUATION VALUE EXCEEDED (PERCENT)
10
1
0.1
0.01
0.001
0.0001
0.00001
0
2
4
6
8
10
ATTENUATION (dB)

FIGURE 21.

The model was used to predict the joint statistics observed by Davidson and Tang (1982) for the Tampa Triad. The single site predictions for Tampa (rain climate zone E) at 19 GHz had an attenuation ratio bias error, $\overline{\nu}$, of -33 percent and an rms deviation in ν of 67 percent. The 11 km joint attenuation statistics were estimated with a bias, $\overline{\nu}$, of 24 percent and and rms deviation of 42 percent. At that spacing, the joint statistics were better estimated than the single site statistics. As the baseline distances increased, the Two-Component model increasingly under-predicted the probabilities at the observed attenuation values (predicted better diversity performance than was observed). For a 16 km spacing, the test statistics were +74 percent for $\overline{\nu}$ and 129 percent for the rms deviation in ν. For a 20 km spacing, the Two-Component model predicted independent occurrences of attenuation events at the two sites at most attenuation levels, a result that was not observed. At this spacing, $\overline{\nu}$ was +307 percent and the rms deviation in ν was 366 percent.

The radar simulations reported by Goldhirsh (1981) compared well with the Two-Component model predictions for short baselines but performed poorly for baselines in excess of 15 km. The results are shown in Figure 20.

Near perfect agreement is evident in this figure for

baselines of 5 km or shorter. The rms deviation in ν was 9.2 percent for the single site predictions. If the CCIR recommendation to set $\nu = 0$ when the attenuation prediction and measurement is within 1 dB, was followed, the rms deviation would have been 0. For the 5 km baseline, $\bar{\nu}$ was 1 percent and the rms deviation in ν was 11 percent, nearly identical with the single site results. For the 10 km baseline, the test statistics show larger deviations between prediction and observation, $\bar{\nu}$ was +21 percent and the rms deviation was 28 percent. By 20 km, the predicted values are close to the values for independent occurrences of attenuation events but, the simulated values were between the 10 km and 35 km baseline results, providing significantly poorer diversity improvement results than predicted by the model.

The radiometer measurements reported by Strickland (1977) were for large baseline separations, in excess of 18 km. The observations and Two-Component model predictions are depicted in Figure 21. The modelled single site statistics are reasonably consistent with the observations. The joint statistics are quite different. The observed behavior for the longer, Ontario diversity baseline was poorer than for the Quebec baseline. These observations do not show the expected improvement in diversity performance with increased baseline for nearly equal orientation angles, β. Strickland attributed the anomolous results to

terrain effects. Such effects would influence the shape of the debris region creating different W_D scales in different horizontal directions.

The available diversity data demonstrate that the simple Two-Component model provides good predictions of diversity performance for short baselines, less than perhaps 15 km, and progressively poorer predictions for longer baselines. The simple model assumed no preferred orientation for the larger debris regions enclosing squall lines and rain bands. Preferred orientations for such storms would produce azimuth dependent W_D vs. R relationships which would significantly affect the performance of the model for large baselines.

5. CONCLUSIONS

The Two-Component model provides a new procedure for the estimation of single path attenuation statistics and joint path (diversity) attenuation statistics for earth-satellite paths to the same satellite. Although applied only to the slant path problem, the model may be readily extended to provide path diversity statistics for terrestrial paths or for mixed slant and terrestrial path problems.

The model performed within the expected deviation bounds as predicted by the Global model (Crane 1980). It performed well both for the prediction of single path and joint path statistics as long as the baseline separation between the paths was less than about 15 km.

The reason for the development of the new model was not to provide competition for existing models such as the recently adopted CCIR model or the Global model but to provide a deeper insight into the meteorological processes responsible for producing attenuation events on one or more propagation paths. This insight is required for the construction of models for the prediction of interference due to rain at attenuating frequencies. The results presented in this papaer represent a first step in the solution of the interference problem. A two or more component model will be required for that task and, if the model cannot produce

adequate results when used to estimate the statistics of processes which have been adequately measured, it will not be acceptable for the estimation of statistics which have not been measured.

The new model was made as simple as possible. Refinements can be made to incorporate the known statistical variations in cell size, rain height and the anticipated variations in debris region scales. These refinements will require a considerably more elaborate computer analysis placing the model calculations out of the range of the programmable pocket calculator.

The new model was developed using only rain gauge and weather radar observations. The utility of the model was demonstraed using observed attenuation statistics. The model includes empirical constants and coefficients whose values were calculated from the meteorological data. Revised coefficients could be obtained which minimize the test statistics for application in selected rain climate regions, selected geographical regions such as Japan, or for a selected type of path such as terrestrial or earth-satellite.

6. REFERENCES

Allnutt, J.E. (1978) "Nature of Space Diversity in Microwave Communications via Geostationary Satellites: A Review", Proc. IEE 125, 369-376.

CCIR, (1982a) "Attenuation by Precipitation and Other Atmospheric Particles", Report 721-1, Study Group 5, Results of the 15 Plenary Assembly, Consultative Committee International Radio, ITU, Geneva.

CCIR, (1982b) "Propagation Data Required for Space Telecommunication Systems", Report 564-2, Study Group 5, Results of the 15 Plenary Assembly, Consultative Committee International Radio, ITU, Geneva.

CCIR, (1982c) "Propagation Data Required for Line-of-Sight Radio-Relay Systems", Report 338-4, Study Group 5, Results of the 15 Plenary Assembly, Consultative Committee International Radio, ITU, Geneva.

Crane, R.K. (1980) "Prediction of Attenuation by Rain", IEEE Trans. Comm. COM-28, 1717-1733.

Crane, R.K. and K.R. Hardy (1980) "The HIPLEX Program in Colby-Goodland, Kansas: 1976-1980", Report No. P-1552-F, Environmental Research & Technology, Inc., Concord, MA, 148 pp.

Crane, R.K. (1979) "Automatic Cell Detection and Tracking", IEEE Trans. Geoscience Elect. GE-17, 250-262.

Crane, R.K. (1977), "Prediction of the Effects of Rain on Satellite Communication Systems", Proc. IEEE 65, 456-474.

Crane, R.K. (1971) "Propagation Phenomena Affecting Satellite Communications Systems Operating in the Centimeter and Millimeter Wavelength Bands", Proc. IEEE 59, 173-188.

Cunningham, R.M. (1952) "Distribution and Growth of Hydrometeon Around a Deep Cyclone", MIT Weather Radar Res. Report 18, MIT Dept. of Meteorology, Cambridge.

Davidson, D. and D.D. Tang (1982) "Diversity Reception of COMSTAR SHF Beacons with the Tampa Triad, 1978-1981", Final Report, GTE Laboratories, Inc., Waltham, MA.

Dutton, E.J. and H.T. Dougherty (1973) "Modeling the Effects of Clouds and Rain Upon Satellite-to-Ground System Performance", Report 73-5, Office of Telecommunications, NTIS No. COM-75-10950, Springfield, VA.

Dutton, E.J., H.K. Kobayaskie, and H.T. Dougherty (1982) "An Improved Model for Earth-Space Microwave Attenuation Distribution Prediction", Radio Science, (this issue).

Fedi, F. (1980) "A Simple Method for Predicting Rain-Attenuation Statistics on Terrestrial and Earth-Space Paths", No. 1B1081, Fondazione Ugo Bordoni, Roma, Italy.

Fedi, F. (1979) "Rainfall Characteristics Across Europe", Alta Frequenza XLVI No. 4, 52E-60E.

Freeney, A.E. and J.D. Gabbe (1969) "A Statistical Description of Intense Rainfall", Bell Syst. Tech. Journal 48, 1789-1851.

Furuhama, Y., H. Ihara, H. Inuki and N. Fugono (1980) "Radar Reflectivity Profile Classified by Rain Type", IECE, Japan, E63.

Goldhirsh, J. (1982) "Radar Prediction of Absolute Rain Fade Distributions for Earth-Satellite Paths and General Methods for Extrapolation of Fade Statistics to Other Locations", IEEE Trans. Antennas and Propagation, (accepted for publication).

Goldhirsh, J. (1981) "Space Diversity Performance Prediction for Earth-Satellite Paths Using Radar Modeling Techniques", S1R81U-044, The Johns Hopkins Univ. Applied Physics Lab., Laurel, MD, 38 pp.

Goldhirsh, J. and I. Katz (1979) "Useful Experimental Results for Earth-Satellite Rain Attenuation Modeling", Trans. IEEE Antennas and Propagation AP-27, 413-415.

Hall, M.P.M. and J.W.F. Goddard (1978) "Variation with Height of the Statistics of Radar Reflectivity due to Hydrometeors", Electronics Letters 14, 7.

Hodge, D.B. (1976) "An Empirical Relationship for Path Diversity Gain", IEEE Trans. Antenna and Propagation AP-24, 250.

Hogg, D.C. (1967) "Path Diversity in Propagation through Rain", IEEE Trans. Antennas and Propagation AP-15, 410-415.

Houze, R. (1981) "Structures of Atmospheric Precipitation Systems - A Global Survey", Radio Science

Ippolito, L.J., R.D. Kaul, and R.G. Wallace (1981) "Propagation Effects Handbook for Satellite Systems Design, A Summary of Propagation Impairments on 10 to 100 GHz Satellite Links with Techniques for System Design", NASA Reference Publication 1082, 2nd ed., NASA Hdqts., 407 pp.

Jones, D.M.A. and A.L. Sims (1978) "Climatology of Instantaneous Rain Rates", Journ. Appl. Meteorol. 17, 1135-1140.

Lin, S.H., H.J. Bergmann, and M.V. Pursley (1980) "Rain Attenuation on Earth-Satellite Paths - Summary of 10-Year Experiments and Studies", Bell Syst. Tech. Journ. 59, 183-228.

Lin, S.H. (1977) "Nationwide Long Term Rain Rate Statistics and Empirical Calculations of 11 GHz Microwave Rain Attenuation", Bell Syst. Tech. Journ. 56, 1581-1604.

Mason, B.J. (1971) The Physics of Clouds, 2nd ed., Clarendon Press.

Misme, P. and J. Fimbel (1975) "Theoretical and Experimental Determination of Attenuation Due to Rain on a Radio-Path", Ann. Telecom. 30, 149-158.

Misme, P. and P. Waldteufel (1980) "A Model for Attenuation by Precipitation on a Microwave Earth-Space Link", Radio Sci. 15, 655-665.

Moupfouma, F. (1981) "Etude de la Pluviometrie et de la Propagation Radioelectrique en Climat Equatorial et Tropical", Ann. de Telecomm., (to be published).

Persinger, R.R., W.L. Stutzman, R.E. Castle and C.W. Bostian (1980) "Millimeter Wave Attenuation Using a Piecewise Uniform Rain Rate Model", IEEE Trans. Antenna and Propagation AP-28, 149-153.

Rice, P.L. and N.R. Holmberg (1973) "Cumulative Time Statistics of Surface - Point Rainfall Rates", IEEE Trans. Comm. COM-21, 1131-1136.

Segal, B. (1979) "High-Intensity Rainfall Statistics for Canada", CRC Report 1329-E, Dept. of Communications, Ottawa, Canada.

Strickland, J.I. (1977) "Radiometrie Measurements of Site Diversity Improvement at Two Canadian Locations", Proc. URSI Commission F Symposium, 29 April - 6 May, LaBaube, France.

Towner, G.C., R.E. Marshall, W.C. Stutzman, C.W. Bostian, T. Pratt, E.A. Manus and P.H. Wiley (1982) "Initial Results from the UPI & SU SIRIO Diversity Experiment", Radio Science (this issue).

Valentin, R. (1977) "Statistiken der Regendäumpfung für Richtfunkverbindungen über 10 GHz", Report 455-TB-62, Deutsche Bundespost Forschungsiustitat beim FTZ, Daumstadt.

APPENDIX

The recently proposed CCIR model (CCIR, 1982b; CCIR, 1982c; Fedi 1981) employs the observed rain rate exceeded 0.01 percent of the year to calculate the attenuation exceeded for the same percentage of the year.

For a terrestrial path (CCIR, 1982c):

$$A_{0.01} = \frac{k(R_{0.01})^{\alpha} D \cdot 90}{(90 + 4D)} \quad \text{(dB)} \qquad \text{(A1)}$$

where $A_{0.01}$ is the attenuation exceeded 0.01 percent of the year, $R_{0.01}$ is the rain rate exceeded 0.01 percent of the year, k, α are the coefficients in the power law relationship between specific attenuation and rain rate and D is the path length.

For an earth-satellite path (CCIR, 1982b):

$$D = \frac{2(H_R - H_o)\cos\theta}{\sqrt{\sin^2\theta + \frac{2(H_R - H_o)}{Re}} + \sin\theta} \quad \text{(km)} \qquad \text{(A2)}$$

$$H_R = 5.1 - 2.15 \log_{10}(1 + 10^{(\theta-27)/25}) \quad \text{(km)}$$

where H_R is the rain height (Figure 10), θ is latitude, H_o is the height of the earth terminal, θ is elevation angle, and the effective path length D is used in equation (A2)

to calculate the effective attenuation at 0.01 percent of the year for an equivalent horizontal path. For a slant path:

$$A_{s,0.01} = A_{0.01}/\cos\ \theta$$

For percentages of the year in the range 0.001 to 0.1,

$$A_P = A_{0.01}\ (P/0.01)^{-\nu}$$

where A_p is the attenuation exceeded P percent of the year and

$$\nu = 0.33 \qquad .001 \leq P \leq .01$$
$$\nu = 0.41 \qquad .01 \leq P \leq .1$$

For a slant path, $A_{s,P} = A_P/\cos\ \theta$.